

Glucoraphanin Ameliorates Obesity and Insulin Resistance Through Adipose Tissue Browning and Reduction of Metabolic Endotoxemia in Mice

メタデータ	言語: eng 出版者: 公開日: 2017-10-03 キーワード (Ja): キーワード (En): 作成者: メールアドレス: 所属:
URL	http://hdl.handle.net/2297/47169

Glucoraphanin ameliorates obesity and insulin resistance through adipose tissue browning
and reduction of metabolic endotoxemia in mice

Running title: Anti-obesity effect of a natural Nrf2 inducer

Naoto Nagata,¹ Liang Xu,¹ Susumu Kohno,² Yusuke Ushida,³ Yudai Aoki,³ Ryohei Umeda,³ Nobuo Fuke,³ Fen Zhuge,¹ Yinhua Ni,¹ Mayumi Nagashimada,¹ Chiaki Takahashi,² Hiroyuki Sukanuma,³ Shuichi Kaneko,⁴ and Tsuguhito Ota^{1,4}

¹Department of Cell Metabolism and Nutrition, Brain/Liver Interface Medicine Research Center, Kanazawa University, Kanazawa, Ishikawa 920-8640, Japan

²Division of Oncology and Molecular Biology, Cancer Research Institute, Kanazawa University, Kanazawa, Ishikawa 920-1192, Japan

³Research and Development Division, Kagome Co., Ltd., 17 Nishitomiya, Nasushiobara, Tochigi 329-2762, Japan

⁴Department of Disease Control and Homeostasis, Kanazawa University Graduate School of Medical Science, Kanazawa, Ishikawa 920-8640, Japan

Corresponding author:

Tsuguhito Ota, M.D., Ph.D.,

Associate Professor, Department of Cell Metabolism and Nutrition,

Brain/Liver Interface Medicine Research Center,

Kanazawa University, Kanazawa, Ishikawa 920-8640, Japan

Phone Number: +81-76-265-2863

Fax Number: +81-76-234-4248

E-mail: tota@staff.kanazawa-u.ac.jp

4554 words
7 figures/1 table

Abstract

Low-grade sustained inflammation links obesity to insulin resistance and nonalcoholic fatty liver disease (NAFLD). However, therapeutic approaches to improve systemic energy balance and chronic inflammation in obesity are limited. Pharmacological activation of nuclear factor (erythroid-derived 2)-like 2 (Nrf2) alleviates obesity and insulin resistance in mice; however, Nrf2 inducers are not clinically available owing to safety concerns. Thus, we examined whether dietary glucoraphanin, a stable precursor of the Nrf2 inducer sulforaphane, ameliorates systemic energy balance, chronic inflammation, insulin resistance, and NAFLD in high-fat diet (HFD)-fed mice. Glucoraphanin supplementation attenuated weight gain, decreased hepatic steatosis, and improved glucose tolerance and insulin sensitivity in HFD-fed wild-type mice but not in HFD-fed Nrf2-knockout mice. Compared with vehicle-treated controls, glucoraphanin-treated HFD-fed mice had lower plasma lipopolysaccharide levels and decreased relative abundance of the Gram-negative bacterial family Desulfovibrionaceae in their gut microbiomes. In HFD-fed mice, glucoraphanin increased energy expenditure and the protein expression of uncoupling protein 1 (Ucp1) in inguinal and epididymal adipose depots. Additionally, in this group, glucoraphanin attenuated hepatic lipogenic gene expression, lipid peroxidation, classically activated M1-like macrophage accumulation, and inflammatory signaling pathways. By promoting fat browning, limiting metabolic endotoxemia-related chronic inflammation, and modulating redox stress, glucoraphanin may mitigate obesity, insulin resistance, and NAFLD.

Low-grade sustained inflammation, triggered by chronically high levels of proinflammatory cytokines and gut microbiota-derived circulatory lipopolysaccharide (LPS), links obesity with comorbidities such as insulin resistance and nonalcoholic fatty liver disease (NAFLD) (1,2). Although a number of pharmacological treatments for obesity and NAFLD have been tested, few drugs are clinically available owing to the lack of long-term efficacy and safety concerns (3,4). Thus, a novel therapeutic approach that would improve energy metabolism and reduce chronic inflammation in obesity is sorely needed.

Nuclear factor (erythroid-derived 2)-like 2 (Nrf2), a basic leucine zipper transcription factor, is widely expressed in human and mouse tissues, and serves as a defense response against extrinsic and intrinsic stressors (5). Upon exposure to electrophilic and oxidative stress, Nrf2 detaches from its repressor, Kelch-like ECH-associated protein 1-nuclear factor (Keap1), and is translocated from the cytoplasm into the nucleus. This translocation leads to the transcriptional activation of genes encoding phase 2 detoxifying and antioxidant enzymes (6). In addition to the ubiquitous induction of cytoprotective genes, Nrf2 regulates a large number of genes involved in glucose and lipid metabolism. In the liver, the constitutive activation of Nrf2 *via* Keap1 knockdown represses the expression of genes involved in gluconeogenesis (7) and lipogenesis (8), thereby alleviating obesity, diabetes, and hepatic steatosis. Accordingly, synthetic Nrf2 inducers such as synthetic triterpenoid 2-cyano-3,12-dioxoolean-1,9-dien-28-oic acid (CDDO)-imidazolide (9), CDDO-methyl ester (known as bardoxolone methyl) (10), and dithiolethione analog, oltipraz (11), have been shown to ameliorate high-fat diet (HFD)-induced obesity and diabetes. These synthetic Nrf2 inducers also decrease liver and adipose tissue lipogenesis,

and enhance glucose uptake in skeletal muscles. However, the mechanisms by which Nrf2 enhances energy metabolism in response to a HFD remain largely unknown. Although enhanced Nrf2 signaling has shown promising results in several animal studies, the synthetic Nrf2 inducers have caused adverse cardiac events and gastrointestinal toxicities in clinical trials (12,13). These observations prompted us to explore a safer Nrf2 inducer for the treatment of obesity, insulin resistance, and NAFLD.

Sulforaphane, an isothiocyanate derived from cruciferous vegetables, is one of the most potent naturally occurring Nrf2 inducers; this compound exhibits anticancer activity in cancer cell lines and in carcinogen-induced rodent models (14). Among the cruciferous vegetables, broccoli sprouts are the best source of glucoraphanin, a stable glucosinolate precursor of sulforaphane (15). In both rodents and humans, glucoraphanin is hydrolyzed by gut microbiota-derived myrosinase into bioactive sulforaphane prior to intestinal absorption (16). A recent clinical study demonstrated the safety of orally administered glucoraphanin (17). In the present study, we examined the dietary glucoraphanin-mediated modulation of systemic energy balance and the mitigation of chronic inflammation, insulin resistance, and NAFLD in diet-induced obese mice.

Research Design and Methods

Glucoraphanin preparation

The sulforaphane precursor, glucoraphanin, was prepared as previously described (17) with minor modifications. Briefly, one day after germination from broccoli seeds (Caudill Seed Company, Louisville, KY), sprouts were boiled in water for 30 min. The

water extract was mixed with dextrinized cornstarch and subsequently spray-dried to yield an extract powder containing 135 mg of glucoraphanin per gram (0.31 mmol/g) (18). The total glucoraphanin titer in the resulting powder was determined by HPLC as previously reported (19).

Mice and diets

Male C57BL/6JSlc mice were purchased from Japan SLC (Hamamatsu, Japan) at 7 weeks of age. Nrf2-knockout (Nrf2^{-/-}) mouse strain (RBRC01390; C57BL/6J background) was provided by RIKEN BRC (Tsukuba, Japan) (6). After a week of acclimation, mice were fed normal chow (NC; containing 2.2% dextrinized cornstarch, 10% kcal from fat, #D12450B; Research Diets, New Brunswick, NJ), NC containing 0.3% glucoraphanin (NC-GR; containing 2.2% extract powder), a high-fat diet (HFD; containing 2.2% dextrinized cornstarch, 60% kcal from fat, #D12492; Research diets), or a HFD containing 0.3% glucoraphanin (HFD-GR; containing 2.2% extract powder) for 14 weeks. Both the NC and the HFD containing cornstarch or glucoraphanin were prepared by Research Diets. All mice studied were maintained on a 12 h light/dark cycle at 24–26°C with free access to water and food. All animal procedures were performed in accordance with the Guidelines for the Care and Use of Laboratory Animals at Kanazawa University, Japan.

Indirect calorimetry

After 3 weeks of feeding, mice were individually housed in an indirect calorimeter chamber at 24–26°C (Oxymax; Columbus Instruments, Columbus, OH). Calorimetry, daily

body weight, and daily food intake data were acquired during a 3-day acclimation period, followed by a 2-day experimental period. Oxygen consumption (VO_2) and carbon dioxide production (VCO_2) were measured in each chamber every 20 minutes. The respiratory exchange ratio ($RER = VCO_2/VO_2$) was calculated using Oxymax software. Energy expenditure was calculated as shown below and normalized to the body mass of each subject.

$$\text{Energy expenditure} = VO_2 \times [3.815 + (1.232 \times RER)]$$

Metabolic measurements and biochemical analyses

Metabolic parameters, body fat composition, insulin sensitivity, and glucose tolerance were assessed as previously described (20). Plasma LPS levels were analyzed using a Limulus amoebocyte lysate assay kit (QCL-1000; Lonza, Allendale, NJ). Plasma LPS binding protein (LBP) levels were determined using an ELISA kit (Enzo Life Sciences, Farmingdale, NY). Immunoblotting was performed with primary antibodies (Supplementary Table 1) as previously described (20). mRNA expression levels were determined by quantitative real-time PCR using SYBR Green with the primers (Supplementary Table 2) as previously described (20).

Isolation and differentiation of inguinal white adipose tissue-derived primary beige adipocytes

Stromal vascular fractions (SVFs) from inguinal white adipose tissue (WAT) of 7-week-old wild-type and $Nrf2^{-/-}$ mice were prepared as previously reported (21). At

confluence, SVF cells were induced for 2 days with differentiation medium containing DMEM/F-12 supplemented with 10% FBS, 20 nM insulin, 1 nM T3, 5 μ M dexamethasone, 500 μ M isobutylmethylxanthine, 125 μ M indomethacin, and 0.5 μ M rosiglitazone (all from Sigma-Aldrich, St. Louis, MO). Induced cells were subsequently cultured in maintenance medium (DMEM/F-12 containing 10% FBS, 20 nM insulin, and 1 nM T3) for 5 days and treated with DMSO or sulforaphane (Toronto Research Chemicals, Toronto, Canada) at the indicated concentrations for 48 h.

Fluorescence-activated cell sorting (FACS)

Cells from the liver and epididymal WAT were prepared as previously described (22). Isolated cells were incubated with Fc-Block (BD Bioscience, San Jose, CA), and subsequently incubated with fluorochrome-conjugated antibodies (Supplementary Table 1). Flow cytometry was performed using a FACS Aria II (BD Bioscience), and the data were analyzed using FlowJo software (Tree Star, Ashland, OR).

Analysis of gut microbiota via pyrosequencing of the 16S rRNA gene

Metagenomic DNA was extracted from mouse cecal content with a QIAamp DNA stool kit (Qiagen, Hilden, Germany). The V1–V2 region of the 16S rRNA gene was amplified using primer sets as previously reported (23). Mixed samples were prepared by pooling approximately equal amounts of PCR amplicons from each sample and subjected to a GS Junior System (Roche Diagnostics, Basel, Switzerland) for subsequent 454 sequencing. Pre-processing and taxonomic assignment of sequencing reads were conducted

as described previously (23) and separated by unique barcodes. The 16S rRNA sequence database was constructed by retrieving 16S sequences of bacterial isolates (1200–2384 bases in length) from the Ribosomal Database Project Release 10.27. We used 4000 filter-passed reads of 16S sequences for the operational taxonomic unit (OTU) analysis of each sample. Clustering of 16S sequence reads with identity scores > 96% into OTUs was performed using UCLUST (www.drive5.com). Representative sequences with identity scores > 96% for each OTU were assigned to bacterial species using BLAST. Principal component analysis using EZR software (<http://www.jichi.ac.jp/saitama-sct/SaitamaHP.files/statmedEN.html>) was applied for assessment of alterations of cecal bacterial phylum associated with diets.

Statistical analyses

Data were expressed as mean \pm SEM. $P < 0.05$ was considered statistically significant. Statistical differences between pairs of groups were determined by a two-tailed Student's *t*-test. An overall difference between more than two groups was determined using a one-way ANOVA. If one-way ANOVAs were significant, differences between individual groups were estimated using a Bonferroni *post hoc* test. All calculations were performed using SPSS Statistics (v19.0, IBM, Armonk, NY).

Results

Glucoraphanin decreases weight gain and adiposity, and increases energy expenditure in high-fat diet (HFD)-fed mice

To investigate the effects of glucoraphanin on systemic energy balance, we examined the body weight of wild-type mice fed normal chow (NC) or a high-fat diet (HFD), supplemented with glucoraphanin or vehicle (i.e., cornstarch only). Glucoraphanin reduced weight gain only in HFD-fed mice without affecting food intake (Fig. 1A and Supplementary Fig. 1A). This reduction was not accompanied by evidence of gross toxicity. We determined the plasma concentration of sulforaphane in NC-GR and HFD-GR mice, but not in NC or HFD mice, indicating that glucoraphanin was absorbed as a sulforaphane following food consumption (Supplementary Fig. 1B). The reduction of weight gain in glucoraphanin-treated HFD-fed mice was largely attributed to the decreased fat mass but not lean mass (Fig. 1B). To assess energy expenditure, we placed the mice in indirect calorimetry cages after 3 weeks of feeding, before an evident change in the body mass of HFD-fed mice was observed (HFD: 29.9 ± 0.5 g vs. HFD-GR: 28.5 ± 0.5 g). Glucoraphanin-treated mice fed the HFD exhibited consistently higher VO_2 and VCO_2 than vehicle-treated HFD-fed controls (Fig. 1C and D), leading to increased energy expenditure (Fig. 1E); however, they displayed similar RER (Fig. 1F), suggesting that glucoraphanin supplementation enhanced sugar and fat use under HFD conditions. On NC-fed mice, glucoraphanin did not affect these parameters of energy balance (Fig. 1B–F). Consistent with increased energy expenditure, glucoraphanin increased the core body temperature of HFD-fed mice by approximately 0.5°C (Fig. 1G).

Glucoraphanin improves diet-induced insulin resistance and glucose tolerance

After 14 weeks of feeding, glucoraphanin supplementation did not affect plasma

triglycerides, total cholesterol, and free fatty acid (FFA) levels in either NC- or HFD-fed mice (Table 1). On NC, blood glucose levels were not altered by glucoraphanin, but on the HFD, glucoraphanin-treated mice exhibited significantly lower fasted blood glucose compared with vehicle-treated controls (Table 1). Additionally, glucoraphanin significantly decreased plasma insulin concentrations in HFD-fed mice under both fasted and fed conditions, resulting in lower homeostatic model assessment-insulin resistance (HOMA-IR; Table 1). During the insulin tolerance test (ITT), glucoraphanin significantly enhanced the reduction in blood glucose levels in HFD-fed mice, but not in NC-fed mice compared with the vehicle-treated controls (Fig. 2A). Glucoraphanin improved glucose tolerance in HFD-fed mice during the glucose tolerance test (GTT), but had no effect on NC-fed mice (Fig. 2B). Insulin secretion during the GTT was not affected by glucoraphanin (data not shown). In line with increased insulin sensitivity, insulin-stimulated Akt phosphorylation on Ser⁴⁷³ was enhanced by glucoraphanin in the liver, muscle, and epididymal WAT of mice fed the HFD (Fig. 2C).

Glucoraphanin does not exert anti-obesity and insulin-sensitizing effects in Nrf2^{-/-} mice

Although the Keap1-Nrf2 pathway is a well-known target of sulforaphane, this isothiocyanate has also been reported to modulate different biological pathways independent of the Keap1-Nrf2 pathway (24,25). To determine whether the anti-obesity and insulin-sensitizing effects of glucoraphanin are mediated through Nrf2, the effects of glucoraphanin on energy balance and glucose metabolism were assessed in NC- and HFD-

fed *Nrf2*^{-/-} mice. Although food intake and plasma concentration of sulforaphane in NC-GR or HFD-GR diet-fed *Nrf2*^{-/-} mice were comparable that detected in wild-type mice fed NC-GR or HFD-GR diet (Supplementary Fig. 1C and D), the effects of glucoraphanin following HFD feeding on weight gain (Fig. 3A), VO_2 (Fig. 3B), VCO_2 (Fig. 3C), energy expenditure (Fig. 3D), RER (Fig. 3E), rectal temperature (Fig. 3F), insulin sensitivity (Fig. 3G), and glucose tolerance (Fig. 3H) were abolished by the *Nrf2* deficiency. These data are consistent with comparable plasma metabolic parameters between glucoraphanin-treated and vehicle-treated mice on the HFD. These metabolic parameters include lipids, blood glucose, insulin, HOMA-IR, and liver enzymes such as alanine transaminase (ALT) and aspartate transaminase (AST) (Supplementary Table 3).

Glucoraphanin blocks HFD-induced reduction of *Ucp1* expression in WAT of wild-type mice but not in *Nrf2*^{-/-} mice

The increased energy expenditure and body temperature of glucoraphanin-treated HFD-fed mice suggest an increase in adaptive thermogenesis. However, glucoraphanin supplementation had little effect on the size and number of lipid droplets in the intrascapular brown adipose tissue (BAT) of HFD-fed wild-type mice (Supplementary Fig. 2A). In addition, the mRNA expression of uncoupling proteins (*Ucps*), PGC-1 α , and deiodinase 2 in BAT and of *Ucps* in skeletal muscle was not altered by glucoraphanin supplementation in both NC- and HFD-fed wild-type mice (Supplementary Fig. 2B and C). In BAT, HFD increased *Ucp1* protein expression, but glucoraphanin did not alter the expression in both wild-type and *Nrf2*^{-/-} mice (Fig. 4A). Brown-like adipocytes expressing

Ucp1, also known as beige cells, exist in various WAT depots and can contribute to thermogenesis (26). Compared with NC, HFD significantly decreased Ucp1 protein levels in epididymal and inguinal WAT of both wild-type and Nrf2^{-/-} mice (Fig. 4A). Glucoraphanin supplementation restored HFD-induced reduction in Ucp1 protein levels in epididymal and inguinal WAT of wild-type mice but not those in Nrf2^{-/-} mice. To examine whether the effects of glucoraphanin were fat cell-autonomous and Nrf2-mediated, we tested the effects of sulforaphane, an active metabolite of glucoraphanin, on the expression of brown fat-selective genes in primary beige adipocytes obtained from inguinal WAT of wild-type and Nrf2^{-/-} mice. In beige adipocytes derived from wild-type mice, treatment with sulforaphane induced the Nrf2 target gene, NAD(P)H:quinone oxidoreductase 1 (*Nqo1*; Fig. 4B) and antioxidant genes (Supplementary Fig. 3A). Concurrently, sulforaphane significantly increased the mRNA expression of brown-fat selective genes, including *Ucp1*, *Prdm16*, *Cidea*, and *Elovl3* (Fig. 4B). In contrast, in Nrf2-deficient beige adipocytes, sulforaphane failed to activate Nrf2 as judged by unaltered mRNA expression of the target genes and to promote the expression of brown-fat selective genes (Supplementary Fig. 3B and Fig. 4C). Importantly, Nrf2-deficient beige adipocytes exhibited less differentiation levels associated with attenuated lipid accumulation (Supplementary Fig. 3C) and lower mRNA expression of fatty acid binding protein 4 (Supplementary Fig. 3C) and brown-fat selective genes compared with wild-type beige adipocytes (Fig. 4C).

Glucoraphanin reduces hepatic steatosis and oxidative stress in HFD-fed mice

The HFD causes hepatic steatosis and inflammation, eventually leading to

steatohepatitis. As shown in Fig. 5A, the increase in liver weight caused by the 14-week-HFD was alleviated by glucoraphanin supplementation. Glucoraphanin also attenuated HFD-induced hepatic steatosis (Fig. 5B). Additionally, compared with the HFD group, the lower levels of plasma ALT, plasma AST, liver triglycerides, and liver FFAs in the HFD-GR group indicate that glucoraphanin alleviated HFD-induced liver damage (Fig. 5C and D). The reduction in hepatic steatosis was accompanied by the decreased expression of the following lipogenic genes: sterol regulatory element binding protein-1c (*Srebf1*), fatty acid synthase (*Fasn*), and peroxisome proliferator-activated receptor gamma (*Pparγ*) (Fig. 5E). Additionally, hepatic levels of malondialdehyde, a marker of lipid peroxidation, were increased by the HFD. Glucoraphanin attenuated lipid peroxidation (Fig. 5F) and decreased gene expression of the NADPH oxidase subunits *gp91^{phox}*, *p22^{phox}*, *p47^{phox}*, and *p67^{phox}* (Fig. 5E). The HFD led to a compensatory increase in the expression of genes involved in fatty acid β-oxidation (*Ppara* and *Cpt1a*) and anti-oxidative stress (*Cat*, *Gpx1*, and *Sod1*) in the liver. However, glucoraphanin did not increase the expression of these genes in the liver of HFD-fed mice further (Fig. 5E).

Glucoraphanin suppresses HFD-induced proinflammatory activation of macrophages in liver and adipose tissue

In response to the HFD, liver-resident macrophages (Kupffer cells) increase the production of proinflammatory cytokines that promote insulin resistance and NAFLD in mice (27). In particular, chemokine (C-C motif) ligand 2 (*Ccl2*) promotes the recruitment of chemokine (C-C motif) receptor 2 (*Ccr2*)-positive monocytic lineages of myeloid cells

into the liver (28). These recruited cells produce a large amount of proinflammatory mediators and activate a lipogenic program (28). Here, we found a prominent induction of tumor necrosis factor- α (*Tnf- α*), *Ccl2*, and *Ccr2* in the liver of HFD-fed mice, which was markedly reduced in glucoraphanin-treated mice (Fig. 6A). Glucoraphanin significantly suppressed HFD-induced inflammatory pathways such as c-Jun N-terminal kinase (JNK) and extracellular signal-regulated kinase (Erk) (Fig. 6B). Glucoraphanin tended to decrease levels of p-NF- κ B p65 (Ser⁵³⁶) in HFD-fed mice, although this decrease was not statistically significant (Fig. 6B). Of note, in the liver of *Nrf2*^{-/-} mice, glucoraphanin failed to suppress HFD-induced inflammatory signal pathways (Supplementary Fig. 4). In addition, glucoraphanin significantly decreased the HFD-induced hepatic expression of macrophage markers, including *F4/80*, *Cd11b*, and *Cd68* (Fig. 6C). Tissue macrophages are phenotypically heterogeneous and have been characterized according to their activation/polarization state as M1-like proinflammatory macrophages or M2-like anti-inflammatory macrophages (29). Consistent with the decreased expression of macrophage markers, glucoraphanin prevented macrophage (F4/80⁺CD11b⁺ cell) accumulation in the liver of HFD-fed mice (Fig. 6D). Additionally, glucoraphanin decreased the number of M1-like liver macrophages expressing surface markers (F4/80⁺CD11b⁺CD11c⁺CD206⁻) (Fig. 6E). In contrast, glucoraphanin increased the number of M2-like liver macrophages (F4/80⁺CD11b⁺CD11c⁻CD206⁺), resulting in a predominantly M2-like macrophage population (Fig. 6E). Moreover, glucoraphanin decreased the mRNA expression of *Tnf- α* and *NADPH oxidase* in the epididymal WAT of HFD-fed mice (Supplementary Fig. 5A). Although the HFD-induced expression of macrophage markers and macrophage

accumulation in epididymal WAT were not altered by glucoraphanin (Supplementary Fig. 5B and C), the number of M1-like macrophages was significantly decreased in the epididymal WAT of glucoraphanin-treated HFD-fed mice (Supplementary Fig. 5D).

Glucoraphanin decreases circulating LPS and the relative abundance of Proteobacteria in the gut microbiomes of HFD-fed mice

Gut microbiota-derived LPS induces chronic inflammation that eventually leads to insulin resistance in obesity, termed metabolic endotoxemia (1,2). Based on our observation that glucoraphanin alleviates inflammation in the liver and epididymal WAT of HFD-fed mice, we subsequently investigated the effects of glucoraphanin on metabolic endotoxemia and gut microbiota. In accordance with previous studies (1,2), the HFD induced a 2-fold increase in circulatory LPS levels, which was reduced by glucoraphanin supplementation (Fig. 7A). Furthermore, plasma and hepatic levels of the LPS marker, LBP, were significantly elevated by the HFD and were reduced by glucoraphanin supplementation (Fig. 7B). A principal component analysis distinguished cecal microbial communities based on diet and treatment, revealing that the metagenomes of HFD-fed mice formed a cluster distinct from the cluster formed by NC-fed mice (Fig. 7C). However, samples from glucoraphanin-treated HFD-fed mice formed a cluster that was indistinguishable from that of vehicle- or glucoraphanin-treated NC-fed mice (Fig. 7C). Importantly, consistent with previous reports (30,31), further analysis at the phylum level demonstrated that the proportion of Gram-negative Proteobacteria was significantly elevated in the gut microbiomes of HFD-fed mice, which was suppressed by glucoraphanin supplementation

(Fig. 7D and E). The increase in the relative abundance of Proteobacteria in HFD-fed mice is mostly explained by an increase in the relative abundance of bacteria from the family Desulfovibrionaceae (Fig. 7F), key producers of endotoxins in animal models of obesity (30). In fact, the relative abundance of Desulfovibrionaceae was positively correlated with plasma LPS levels (Fig. 7G). Furthermore, plasma LPS levels were significantly and positively correlated with the hepatic mRNA levels of *Tnf- α* , *gp91^{phox}*, and *F4/80* (Fig. 7H). Similarly, the liver expression of other marker genes was both significantly and positively correlated with plasma LPS levels and with one another (Supplementary Table 4).

Discussion

In the present study, we demonstrated that glucoraphanin, a stable precursor of the Nrf2 inducer sulforaphane, mitigated HFD-induced weight gain, insulin resistance, hepatic steatosis, oxidative stress, and chronic inflammation in mice. The weight-reducing and insulin-sensitizing effects of glucoraphanin were abolished in Nrf2^{-/-} mice. Additionally, glucoraphanin lowered plasma LPS levels in HFD-fed mice, and decreased the relative abundance of Desulfovibrionaceae. At the molecular level, glucoraphanin increased Ucp1 protein expression in WAT depots, while suppressing the hepatic mRNA expression of genes involved in lipogenesis, NADPH oxidase, and inflammatory cytokines. Our data suggest that in diet-induced obese mice, glucoraphanin restores energy expenditure and limits gut-derived metabolic endotoxemia, thereby preventing hepatic steatosis, insulin resistance, and chronic inflammation.

Consistent with previous reports demonstrating the anti-obesity effects of synthetic

Nrf2 inducers (9–11), we show that the oral administration of glucoraphanin mitigates HFD-induced weight gain (Fig. 1A). The dose of glucoraphanin used in the current study (about 12 $\mu\text{mol}/\text{mouse}/\text{day}$) is similar to that used in other experiments investigating its antitumor effects in mice (14,32,33). Here, we show that the effect of glucoraphanin on whole-body energy expenditure and the protein expression of Ucp1 in WAT were abolished in Nrf2^{-/-} mice (Fig. 3D and 4A). A recent study using adipocyte-specific PRDM16-deficient mice indicated that adaptive thermogenesis in beige fat also contributes to systemic energy expenditure (26). The mutant mice in the aforementioned study, which exhibited markedly reduced *Ucp1* mRNA expression in inguinal WAT and minimal effects on BAT, developed obesity and insulin resistance in response to a HFD. Thus, we believe that the increased energy expenditure in glucoraphanin-treated HFD-fed mice stems from, at least in part, an increase in beige fat, even though the expression of *Ucps* in BAT and skeletal muscle is not altered. Further analysis using Ucp1-knockout mice will elucidate the relative contribution of beige fat to the Nrf2-mediated metabolic effects elicited by glucoraphanin.

Several studies indicated that Nrf2^{-/-} mice are partially protected from HFD-induced obesity and associated with milder insulin resistance compared with wild-type counterparts (9,34,35). Recently, Schneider *et al.* demonstrated that mitigation of HFD-induced obesity in Nrf2^{-/-} mice, which was 25% less body weight than that of wild-type mice after 6 weeks of feeding (35). They also found that HFD-fed Nrf2^{-/-} mice exhibit a 20–30% increase in energy expenditure that is associated with an approximately 3-fold up-regulation of Ucp1 protein expression in abdominal WAT (35). In the present study, Nrf2^{-/-} mice gained less

weight after 6 weeks of HFD feeding compared with HFD-fed wild-type mice (Figure 1A and 3A; Nrf2^{-/-}: 35.9 ± 0.9 g vs. wild-type: 39.0 ± 0.8 g, $P < 0.05$). The lower body mass of Nrf2^{-/-} mice raises the possibility that anti-obesity effect of glucoraphanin was completely phenocopied by Nrf2 gene deficiency. However, several observations suggest that Nrf2^{-/-} mice only partially phenocopy the effect of glucoraphanin on weight gain reduction. 1) In the present study, the weight difference between Nrf2^{-/-} and wild-type mice was only 8%, which is much less than that in the previous study (35). 2) In Nrf2^{-/-} mice, compared with NC, HFD induced significant weight gain (Fig. 3A), glucose intolerance (Fig. 3H), and insulin resistance as judged by increased HOMA-IR (Supplementary Table 3). 3) Metabolic rate and energy expenditure of Nrf2^{-/-} mice were comparable with those in wild-type mice (Fig. 1C–E and 3B–D). 4) Ucp1 protein levels in both epididymal WAT and inguinal WAT of HFD-fed Nrf2^{-/-} mice were lower than those in HFD-GR-fed wild-type mice (Fig. 4A). Taken together, these findings suggest that Nrf2 gene deficiency is not sufficient to block HFD-induced obesity by increasing energy expenditure and Ucp1 expression in WAT depots, and to mask the effect of glucoraphanin. However, we cannot fully exclude the possibility that the effects of glucoraphanin are mediated by Nrf2 independent-mechanisms. Possible reasons for the discordance in metabolic phenotypes of Nrf2^{-/-} between the previous study (35) and ours may be due to differences in knockout mouse lines and experimental conditions (e.g. age of mice at beginning of HFD feeding, composition of HFD, and temperature in the metabolic chamber).

Our *in vitro* study of primary beige adipocytes revealed that sulforaphane promotes the expression of brown-fat selective genes (Fig. 4B). Importantly, the concentration of

sulforaphane used in cell culture (0.2–5 μM) is comparable with that detected in mice fed NC-GR and HFD-GR diet (Supplementary Fig. 1B). Moreover, we determined that Nrf2 acts as a positive regulator of beige adipocyte differentiation (Fig. 4C and Supplementary Fig. 3C). The less differentiation levels in Nrf2-deficient beige adipocytes are in agreement with previous reports demonstrating Nrf2 induces white adipocyte differentiation through increasing the gene expression of *Ppar γ* (34) and *Cebp β* (36), common transcription factors regulating the differentiation of brown, beige, and white adipocytes. Furthermore, it is noteworthy that Nrf2 has been reported to bind NF-E2-binding sites in the 5'-flanking region of the human and rodent *Ucp1* genes (37). However, we cannot exclude the possibilities that glucoraphanin affects sympathetic nervous activity or that hormonal factors are regulating fat browning (38). In addition, mitochondrial reactive oxidative species facilitate *Ucp1*-dependent respiration in BAT and whole-body energy expenditure by promoting the sulfenylation of a specific cysteine residue (Cys253) in *Ucp1* (39). The molecular mechanism by which Nrf2 regulates the expression and thermogenic activity of *Ucp1* in beige adipocytes requires further investigation.

Glucoraphanin supplementation improved the systemic glucose tolerance and insulin sensitivity of HFD-fed mice. Although the molecular mechanism by which synthetic Nrf2 inducers enhance glucose uptake is unclear, AMP-activated protein kinase (AMPK) activation may mediate this enhancement in mouse skeletal muscle and adipose tissue (9–11). The phosphorylation levels of AMPK (Thr¹⁷²) and acetyl-CoA carboxylase (Ser⁷⁹) in peripheral insulin target tissues were comparable between glucoraphanin-treated NC- and HFD-fed mice and vehicle-treated controls (Supplementary Fig. 6). These data suggest that

AMPK activation is not necessary for glucoraphanin to exert its insulin-sensitizing effect on HFD-fed mice. Additional studies using the hyperinsulinemic-euglycemic clamp technique are needed to determine which tissues contribute to the insulin-sensitizing effects of glucoraphanin.

The beneficial effects of glucoraphanin on hepatic lipid metabolism were not accompanied by AMPK activation or the increased expression of fatty acid β -oxidation genes (Fig. 5E). Instead, glucoraphanin mitigated HFD-induced oxidative stress and inflammation in the liver. In obesity, hepatic inflammation mediated by macrophage/monocyte-derived proinflammatory cytokines promotes lipogenesis through the inhibition of insulin signaling and SREBP activation (40,41). In fact, the depletion of Kupffer cells by clodronate liposomes ameliorates hepatic steatosis and insulin sensitivity in HFD-fed mice (27). Furthermore, *Ccl2*- or *Ccr2*-deficient mice are protected from diet-induced hepatic steatosis even though they still become obese (42,43). Moreover, the specific ablation of M1-like macrophages restores insulin sensitivity in diet-induced obese mice (44), while the deletion of *Ppar δ* , which promotes M2 activation, predisposes lean mice to develop insulin resistance (45). Therefore, decreased hepatic macrophage accumulation and M2-dominant polarization of hepatic and adipose macrophages account, at least in part, for the protection from hepatic steatosis and insulin resistance in glucoraphanin-treated HFD-fed mice.

One of the most important findings of this study is that glucoraphanin decreases the relative abundance of Gram-negative Proteobacteria, particularly family Desulfovibrionaceae, while reducing circulatory LPS levels (Fig. 7). Recent studies

demonstrated that a significant increase in Desulfovibrionaceae, potential endotoxin producers, in the gut microbiomes of both HFD-induced obese mice and obese human subjects compared to lean individuals (30,31,46). We cannot exclude the possibility that other microbiota-derived products, such as bile acids and short chain fatty acids, also mediate the metabolic action of glucoraphanin. Whether the interaction between sulforaphane and gut microbiota is affected directly or indirectly by altered host physiology remains to be determined. However, several studies have suggested that sulforaphane can alter the gut microbiota directly, as isothiocyanates (including sulforaphane) have been shown to exhibit antibacterial activity against Proteobacteria (47,48). This activity may proceed *via* redox disruption and enzyme denaturation reactions involving the isothiocyanate reactive group, $-N=C=S$, the thiol group (-SH) of glutathione and proteobacterial proteins (47,48). Additionally, sulforaphane exhibits antibacterial activity against *Helicobacter pylori*, a member of the phylum Proteobacteria (49). We are unaware of any previous reports demonstrating that isothiocyanates inhibit the proliferation of Desulfovibrionaceae. The mechanistic underpinnings of this antibacterial activity require elucidation.

In conclusion, the results of the present study indicate that glucoraphanin may be effective in preventing obesity and related metabolic disorders such as NAFLD and type 2 diabetes. A recent clinical study demonstrated that supplementation with a dietary dose of glucoraphanin (69 $\mu\text{mol/day}$) for two months significantly decreased the plasma liver enzymes, ALT and AST, although body mass did not change (18). Long-term treatment with a higher dose of glucoraphanin (800 $\mu\text{mol/day}$), which can be safely administered

without any harmful side effects (17), may be required to achieve an anti-obesity effect in humans.

Author contributions

N.N. collected data and wrote the manuscript. Y.U., Y.A., and R.U. collected data and edited the manuscript. L.X., S.K., N.F., F.Z., Y.N., and M.N. collected data. C.T., H.S., and S.K. contributed to discussion and reviewed the manuscript. T.O. contributed to discussion, reviewed the manuscript, and edited the manuscript. T.O. is the guarantor of this work and, as such, had full access to all study data and takes responsibility for the integrity of the data and the accuracy of the data analysis.

Acknowledgments

This work was supported by Japan Society for the Promotion of Science KAKENHI, Grant Numbers 15K00813 (N.N.), 15K12698 (T.O.), and 16H03035 (T.O.). There are no potential conflicts of interest to declare.

Parts of this article was presented (number 1924-P) at the 76th Scientific Sessions of the American Diabetes Association, New Orleans, LA, 10-14 June 2016.

We would also like to thank M. Nakayama and K. Hara (Kanazawa University) for their technical assistance. Finally, we would like to thank Editage (www.editage.jp) for English language editing.

References

1. Cani PD, Amar J, Iglesias MA, Poggi M, Knauf C, Bastelica D, Neyrinck AM, Fava F, Tuohy KM, Chabo C, Waget A, Delmée E, Cousin B, Sulpice T, Chamontin B, Ferrières J, Tanti JF, Gibson GR, Casteilla L, Delzenne NM, Alessi MC, Burcelin R. Metabolic endotoxemia initiates obesity and insulin resistance. *Diabetes* 2007;56:1761–1772
2. Cani PD, Bibiloni R, Knauf C, Waget A, Neyrinck AM, Delzenne NM, Burcelin R. Changes in gut microbiota control metabolic diet-induced obesity and diabetes in mice. *Diabetes* 2008;57:1470–1481
3. Dietrich MO, Horvath TL. Limitations in anti-obesity drug development: the critical role of hunger-promoting neurons. *Nat Rev Drug Discov* 2012;11:675–691
4. Sanyal AJ, Chalasani N, Kowdley KV, McCullough A, Diehl AM, Bass NM, Neuschwander-Tetri BA, Lavine JE, Tonascia J, Unalp A, Van Natta M, Clark J, Brunt EM, Kleiner DE, Hoofnagle JH, Robuck PR; NASH CRN. Pioglitazone, vitamin E, or placebo for nonalcoholic steatohepatitis. *N Engl J Med* 2010;362:1675–1685
5. Motohashi H, Yamamoto M. Nrf2-Keap1 defines a physiologically important stress response mechanism. *Trends Mol Med* 2004;10:549–557
6. Itoh K, Chiba T, Takahashi S, Ishii T, Igarashi K, Katoh Y, Oyake T, Hayashi N, Satoh K, Hatayama I, Yamamoto M, Nabeshima Y. An Nrf2/small Maf heterodimer mediates the induction of phase II detoxifying enzyme genes through antioxidant response elements. *Biochem Biophys Res Commun* 1997;236:313–322
7. Uruno A, Furusawa Y, Yagishita Y, Fukutomi T, Muramatsu H, Negishi T, Sugawara A, Kensler TW, Yamamoto M. The keap1-nrf2 system prevents onset of diabetes mellitus. *Mol Cell Biol* 2013;33:2996–3010
8. Yates MS, Tran QT, Dolan PM, Osburn WO, Shin S, McCulloch CC, Silkworth JB, Taguchi K, Yamamoto M, Williams CR, Liby KT, Sporn MB, Sutter TR, Kensler TW. Genetic versus chemoprotective activation of Nrf2 signaling: overlapping yet distinct gene expression profiles between Keap1 knockout and triterpenoid-treated mice. *Carcinogenesis* 2009;30:1024–1031
9. Shin S, Wakabayashi J, Yates MS, Wakabayashi N, Dolan PM, Aja S, Liby KT, Sporn MB, Yamamoto M, Kensler TW. Role of Nrf2 in prevention of high-fat diet-induced obesity by synthetic triterpenoid CDDO-imidazolide. *Eur J Pharmacol* 2009;620:138–144
10. Saha PK, Reddy VT, Konopleva M, Andreeff M, Chan L. The triterpenoid 2-cyano-3,12-dioxooleana-1,9-dien-28-oic-acid methyl ester has potent anti-diabetic effects in diet-induced diabetic mice and Lepr(db/db) mice. *J Biol Chem* 2010;285:40581–40592
11. Yu Z, Shao W, Chiang Y, Foltz W, Zhang Z, Ling W, Fantus IG, Jin T. Oltipraz upregulates the nuclear factor (erythroid-derived 2)-like 2 [corrected](NRF2) antioxidant system and prevents insulin resistance and obesity induced by a high-fat diet in C57BL/6J mice. *Diabetologia* 2011;54:922–934
12. de Zeeuw D, Akizawa T, Audhya P, Bakris GL, Chin M, Christ-Schmidt H,

- Goldsberry A, Houser M, Krauth M, Lambers Heerspink HJ, McMurray JJ, Meyer CJ, Parving HH, Remuzzi G, Toto RD, Vaziri ND, Wanner C, Wittes J, Wrolstad D, Chertow GM; BEACON Trial Investigators. Bardoxolone methyl in type 2 diabetes and stage 4 chronic kidney disease. *N Engl J Med* 2013;369:2492–2503
13. Kelley MJ, Glaser EM, Herndon JE 2nd, Becker F, Bhagat R, Zhang YJ, Santella RM, Carmella SG, Hecht SS, Gallot L, Schilder L, Crowell JA, Perloff M, Folz RJ, Bergan RC. Safety and Efficacy of Weekly Oral Oltipraz in Chronic Smokers. *Cancer Epidemiol Biomarkers Prev* 2005;14:892–899
 14. Fahey JW, Zhang Y, Talalay P. Broccoli sprouts: an exceptionally rich source of inducers of enzymes that protect against chemical carcinogens. *Proc Natl Acad Sci U S A* 1997;94:10367–10372
 15. Zhang Y, Talalay P, Cho CG, Posner GH. A major inducer of anticarcinogenic protective enzymes from broccoli: isolation and elucidation of structure. *Proc Natl Acad Sci U S A* 1992;89:2399–2403
 16. Shapiro TA, Fahey JW, Wade KL, Stephenson KK, Talalay P. Human metabolism and excretion of cancer chemoprotective glucosinolates and isothiocyanates of cruciferous vegetables. *Cancer Epidemiol Biomarkers Prev*, 1998;7:1091–1100
 17. Kensler TW, Ng D, Carmella SG, Chen M, Jacobson LP, Muñoz A, Egner PA, Chen JG, Qian GS, Chen TY, Fahey JW, Talalay P, Groopman JD, Yuan JM, Hecht SS. Modulation of the metabolism of airborne pollutants by glucoraphanin-rich and sulforaphane-rich broccoli sprout beverages in Qidong, China. *Carcinogenesis* 2012;33:101–107
 18. Kikuchi M, Ushida Y, Shiozawa H, Umeda R, Tsuruya K, Aoki Y, Suganuma H, Nishizaki Y. Sulforaphane-rich broccoli sprout extract improves hepatic abnormalities in male subjects. *World J Gastroenterol* 2015;21:12457–12467
 19. Wade KL, Garrard IJ, Fahey JW. Improved hydrophilic interaction chromatography method for the identification and quantification of glucosinolates. *J Chromatogr A* 2007;1154:469–472
 20. Nagata N, Matsuo K, Bettaieb A, Bakke J, Matsuo I, Graham J, Xi Y, Liu S, Tomilov A, Tomilova N, Gray S, Jung DY, Ramsey JJ, Kim JK, Cortopassi G, Havel PJ, Haj FG. Hepatic Src homology phosphatase 2 regulates energy balance in mice. *Endocrinology* 2012;153:3158–3169
 21. Aune UL, Ruiz L, Kajimura S. Isolation and differentiation of stromal vascular cells to beige/brite cells. *J Vis Exp* 2013;(73), e50191. DOI: 10.3791/50191
 22. Kitade H, Sawamoto K, Nagashimada M, Inoue H, Yamamoto Y, Sai Y, Takamura T, Yamamoto H, Miyamoto K, Ginsberg HN, Mukaida N, Kaneko S, Ota T. CCR5 plays a critical role in obesity-induced adipose tissue inflammation and insulin resistance by regulating both macrophage recruitment and M1/M2 status. *Diabetes* 2012;61:1680–1690
 23. Kim SW, Suda W, Kim S, Oshima K, Fukuda S, Ohno H, Morita H, Hattori M. Robustness of gut microbiota of healthy adults in response to probiotic intervention revealed by high-throughput pyrosequencing. *DNA Res* 2013;20:241–253
 24. Greaney AJ, Maier NK, Leppla SH, Moayeri M. Sulforaphane inhibits multiple inflammasomes through an Nrf2-independent mechanism. *J Leukoc Biol*

- 2016;99:189–199
25. Myzak MC, Karplus PA, Chung FL, Dashwood RH. A novel mechanism of chemoprotection by sulforaphane: inhibition of histone deacetylase. *Cancer Res* 2004;64:5767–5774
 26. Cohen P, Levy JD, Zhang Y, Frontini A, Kolodin DP, Svensson KJ, Lo JC, Zeng X, Ye L, Khandekar MJ, Wu J, Gunawardana SC, Banks AS, Camporez JP, Jurczak MJ, Kajimura S, Piston DW, Mathis D, Cinti S, Shulman GI, Seale P, Spiegelman BM. Ablation of PRDM16 and beige adipose causes metabolic dysfunction and a subcutaneous to visceral fat switch. *Cell* 2014;156:304–316
 27. Huang W, Metlakunta A, Dedousis N, Zhang P, Sipula I, Dube JJ, Scott DK, O'Doherty RM. Depletion of liver Kupffer cells prevents the development of diet-induced hepatic steatosis and insulin resistance. *Diabetes* 2010;59:347–357
 28. Obstfeld AE, Sugaru E, Thearle M, Francisco AM, Gayet C, Ginsberg HN, Ables EV, Ferrante AW Jr. C-C chemokine receptor 2 (CCR2) regulates the hepatic recruitment of myeloid cells that promote obesity-induced hepatic steatosis. *Diabetes* 2010;59:916–925
 29. Mantovani A, Sica A, Sozzani S, Allavena P, Vecchi A, Locati M. The chemokine system in diverse forms of macrophage activation and polarization. *Trends Immunol* 2004;25:677–686
 30. Zhang C, Zhang M, Wang S, Han R, Cao Y, Hua W, Mao Y, Zhang X, Pang X, Wei C, Zhao G, Chen Y, Zhao L. Interactions between gut microbiota, host genetics and diet relevant to development of metabolic syndromes in mice. *ISME J* 2010;4:232–241
 31. Hildebrandt MA, Hoffmann C, Sherrill-Mix SA, Keilbaugh SA, Hamady M, Chen YY, Knight R, Ahima RS, Bushman F, Wu GD. High-fat diet determines the composition of the murine gut microbiome independently of obesity. *Gastroenterology* 2009;137:1716–1724
 32. Conaway CC, Wang CX, Pittman B, Yang YM, Schwartz JE, Tian D, McIntee EJ, Hecht SS, Chung FL. Phenethyl isothiocyanate and sulforaphane and their N-acetylcysteine conjugates inhibit malignant progression of lung adenomas induced by tobacco carcinogens in A/J mice. *Cancer Res* 2005;65:8548–8557
 33. Shen G, Khor TO, Hu R, Yu S, Nair S, Ho CT, Reddy BS, Huang MT, Newmark HL, Kong AN. Chemoprevention of familial adenomatous polyposis by natural dietary compounds sulforaphane and dibenzoylmethane alone and in combination in *ApcMin/+* mouse. *Cancer Res* 2007;67:9937–9944
 34. Pi J, Leung L, Xue P, Wang W, Hou Y, Liu D, Yehuda-Shnaidman E, Lee C, Lau J, Kurtz TW, Chan JY. Deficiency in the nuclear factor E2-related factor-2 transcription factor results in impaired adipogenesis and protects against diet-induced obesity. *J Biol Chem* 2010;285:9292–9300
 35. Schneider K, Valdez J, Nguyen J, Vawter M, Galke B, Kurtz TW, Chan JY. Increased Energy Expenditure, *Ucp1* Expression, and Resistance to Diet-induced Obesity in Mice Lacking Nuclear Factor-Erythroid-2-related Transcription Factor-2 (Nrf2). *J Biol Chem* 2016;291:7754–7766
 36. Hou Y, Xue P, Bai Y, Liu D, Woods CG, Yarborough K, Fu J, Zhang Q, Sun G,

- Collins S, Chan JY, Yamamoto M, Andersen ME, Pi J. Nuclear factor erythroid-derived factor 2-related factor 2 regulates transcription of CCAAT/enhancer-binding protein β during adipogenesis. *Free Radic Biol Med* 2012;52:462–472.
37. Rim JS, Kozak LP. Regulatory motifs for CREB-binding protein and Nfe2l2 transcription factors in the upstream enhancer of the mitochondrial uncoupling protein 1 gene. *J Biol Chem* 2002;277:34589–34600
 38. Kajimura S, Spiegelman BM, Seale P. Brown and beige fat: Physiological roles beyond heat generation. *Cell Metab* 2015;22:546–559
 39. Chouchani ET, Kazak L, Jedrychowski MP, Lu GZ, Erickson BK, Szpyt J, Pierce KA, Laznik-Bogoslavski D, Vetrivelan R, Clish CB, Robinson AJ, Gygi SP, Spiegelman BM. Mitochondrial ROS regulate thermogenic energy expenditure and sulfenylation of UCP1. *Nature* 2016;532:112–116.
 40. Ma KL, Ruan XZ, Powis SH, Chen Y, Moorhead JF, Varghese Z. Inflammatory stress exacerbates lipid accumulation in hepatic cells and fatty livers of apolipoprotein E knockout mice. *Hepatology* 2008;48:770–781
 41. Lawler JF Jr, Yin M, Diehl AM, Roberts E, Chatterjee S. Tumor necrosis factor- α stimulates the maturation of sterol regulatory element binding protein-1 in human hepatocytes through the action of neutral sphingomyelinase. *J Biol Chem* 1998;273:5053–5059
 42. Kanda H, Tateya S, Tamori Y, Kotani K, Hiasa KI, Kitazawa R, Kitazawa S, Miyachi H, Maeda S, Egashira K, Kasuga M. MCP-1 contributes to macrophage infiltration into adipose tissue, insulin resistance, and hepatic steatosis in obesity. *J Clin Invest* 2006;116:1494–1505
 43. Weisberg SP, Hunter D, Huber R, Lemieux J, Slaymaker S, Vaddi K, Charo I, Leibel RL, Ferrante AW Jr. CCR2 modulates inflammatory and metabolic effects of high-fat feeding. *J Clin Invest* 2006;116:115–124
 44. Patsouris D, Li PP, Thapar D, Chapman J, Olefsky JM, Neels JG. Ablation of CD11c-positive cells normalizes insulin sensitivity in obese insulin resistant animals. *Cell Metab* 2008;8:301–309
 45. Odegaard JI, Ricardo-Gonzalez RR, Red Eagle A, Vats D, Morel CR, Goforth MH, Subramanian V, Mukundan L, Ferrante AW, Chawla A. Alternative M2 activation of Kupffer cells by PPAR δ ameliorates obesity-induced insulin resistance. *Cell Metab* 2008;7:496–507
 46. Xiao S, Fei N, Pang X, Shen J, Wang L, Zhang B, Zhang M, Zhang X, Zhang C, Li M, Sun L, Xue Z, Wang J, Feng J, Yan F, Zhao N, Liu J, Long W, Zhao L. A gut microbiota-targeted dietary intervention for amelioration of chronic inflammation underlying metabolic syndrome. *FEMS Microbiol Ecol* 2014;87:357–367
 47. Aires A, Mota VR, Saavedra MJ, Rosa EA, Bennett RN. The antimicrobial effects of glucosinolates and their respective enzymatic hydrolysis products on bacteria isolated from the human intestinal tract. *J Appl Microbiol* 2009;106:2086–2095
 48. Sofrata A, Santangelo EM, Azeem M, Borg-Karlson A-K, Gustafsson A, Pütsep K. Benzyl isothiocyanate, a major component from the roots of *Salvadora persica* is highly active against Gram-negative bacteria. *PLoS One* 2011;6:e23045
 49. Fahey JW, Haristoy X, Dolan PM, Kensler TW, Scholtus I, Stephenson KK, Talalay

P, Lozniewski A. Sulforaphane inhibits extracellular, intracellular, and antibiotic-resistant strains of *Helicobacter pylori* and prevents benzo[a]pyrene-induced stomach tumors. Proc Natl Acad Sci U S A 2002;99:7610–7615

Table 1 Metabolic parameters in fed and fasted mice

	NC	NC-GR	HFD	HFD-GR
Plasma TG (mg/dL)	139.2 ± 9.4	140.7 ± 8.1	144.6 ± 5.4	123.6 ± 9.2
Plasma TC (mg/dL)	161.2 ± 7.7	161.4 ± 3.5	212.6 ± 2.1**	210.2 ± 1.8**
Plasma FFAs (mmol/L)	0.85 ± 0.07	0.96 ± 0.07	0.93 ± 0.05	0.81 ± 0.05
Blood glucose (mg/dL)				
Fed	126 ± 6	124 ± 3	152 ± 4**	145 ± 4*
Fasted	77 ± 3	76 ± 3	131 ± 9**	94 ± 5###
Plasma insulin (ng/mL)				
Fed	1.4 ± 0.2	1.0 ± 0.2	5.3 ± 0.5**	3.6 ± 0.4**#
Fasted	0.2 ± 0.0	0.1 ± 0.0	2.2 ± 0.2**	1.3 ± 0.2**###
HOMA-IR	1.0 ± 0.1	0.6 ± 0.2	17.7 ± 1.6**	8.0 ± 1.3**###

Shown are blood glucose and plasma insulin levels of mice fed (*ad libitum*) or fasted for 16 h. Plasma triglyceride (TG), total cholesterol (TC), and free fatty acids (FFAs) were measured in fasting plasma. Measurements are reported as mean ± SEM (n = 9/group). **P* < 0.05, ***P* < 0.01 vs. NC; #*P* < 0.05, ###*P* < 0.01 vs. HFD. NC: normal chow, HFD: high-fat diet, GR: glucoraphanin, HOMA-IR: homeostasis model assessment of insulin resistance.

Figure legends

Figure 1—Glucoraphanin reduces weight gain and increases energy expenditure in high-fat diet (HFD)-fed mice. *A*: Body weight of mice fed normal chow (NC; white circles), chow with glucoraphanin (NC-GR; black circles), a high-fat diet (HFD; white triangles), or HFD with glucoraphanin (HFD-GR; black triangles) ($n = 9/\text{group}$). *B*: Representative computed tomographic images of abdominal regions of mice fed the indicated diet for 13 weeks. Pink and yellow areas represent visceral and subcutaneous fat, respectively. Bar graphs represent body fat mass and lean mass calculated from the CT scan data. Oxygen consumption (*C*; VO_2), carbon dioxide production (*D*; VCO_2), energy expenditure (*E*), and respiratory exchange ratio (*F*; RER) during light and dark cycles in mice fed the indicated diet for 3 weeks. *G*: Rectal temperature in mice fed the indicated diet for 6 weeks. Data are presented as mean \pm SEM. $*P < 0.05$, $**P < 0.01$ vs. NC; $\#P < 0.05$, $\#\#P < 0.01$ vs. HFD.

Figure 2—Glucoraphanin improves insulin sensitivity and glucose tolerance in HFD-fed mice. *A*: Insulin tolerance test (ITT, 0.9 U/kg body weight for NC and NC-GR mice; 1.2 U/kg body weight for HFD and HFD-GR mice) after 11 weeks of feeding ($n = 9/\text{group}$). *B*: Glucose tolerance test (GTT, 2 g/kg body weight) after 9 weeks ($n = 9/\text{group}$). Bar graphs represent AUC calculations. *C*: Mice on the indicated diet for 14 weeks were injected intraperitoneally with saline ($n = 2/\text{group}$) or insulin ($n = 6/\text{group}$, 10 U/kg body weight), and sacrificed 10 min after injection. Total liver, quadriceps muscle, and epididymal adipose depot (eWAT) lysates were immunoblotted for pS473-Akt and Akt, quantitated,

and presented as mean \pm SEM. * P < 0.05, ** P < 0.01 vs. NC; # P < 0.05, ## P < 0.01 vs. HFD. A.U.: arbitrary unit.

Figure 3—The anti-obesity and insulin sensitizing effects of glucoraphanin are abolished in $Nrf2^{-/-}$ mice. *A*: Body weight of $Nrf2^{-/-}$ mice fed normal chow (NC; white circles), chow with glucoraphanin (NC-GR; black circles), a high-fat diet (HFD; white triangles), or HFD with glucoraphanin (HFD-GR; black triangles) for 14 weeks. *B*, *C*, *D*, *E*: VO_2 (*B*), VCO_2 (*C*), energy expenditure (*D*), respiratory exchange ratio (*E*; RER) of $Nrf2^{-/-}$ mice fed the indicated diet for 3 weeks. *F*: Rectal temperature in mice $Nrf2^{-/-}$ fed the indicated diet for 6 weeks. ITT (0.9 U/kg body weight for NC and NC-GR mice; 1.2 U/kg body weight for HFD and HFD-GR mice) (*G*) and GTT (2 g/kg body weight) (*H*) were performed after 9 and 11 weeks of feeding, respectively. Bar graphs represent AUC calculations. Data are presented as mean \pm SEM (NC: $n = 8$, NC-GR: $n = 8$, HFD: $n = 10$, HFD-GR: $n = 8$). * P < 0.05, ** P < 0.01 vs. NC.

Figure 4—Glucoraphanin blocks HFD-induced reduction of uncoupling protein-1 (Ucp1) protein levels in white adipose depots of wild-type mice but not in $Nrf2$ -knockout ($Nrf2^{-/-}$) mice. *A*: Shown are immunoblot analyses of Ucp1 and Tubulin expression using lysates of brown adipose tissue (BAT; 0.5 μ g protein), epididymal fat depots (eWAT; 5 μ g protein), and inguinal fat depots (ingWAT; 2 μ g protein) from wild-type or $Nrf2^{-/-}$ mice on the indicated diet for 14 weeks. Bar graphs represent normalized data of Ucp1/Tubulin from four independent blots, and are presented as mean \pm SEM ($n = 8$ /group). * P < 0.05, ** P <

0.01 vs. NC-fed wild-type or NC-fed *Nrf2*^{-/-} mice; ###*P* < 0.01 vs. HFD-fed wild-type mice. *B*: Quantitative real-time PCR determination of mRNA levels of *Nqo1* and of genes involved in fat browning in the absence or presence of sulforaphane (SFN; 0.2, 1, 2, or 5 μ M) in primary beige adipocytes isolated from inguinal WAT of wild-type mice (normalized against *36B4*). Bar graphs represent mean \pm SEM (n = 6/group). *C*: The same experiment as in (*B*) was repeated with primary beige adipocytes isolated from ingWAT of *Nrf2*^{-/-} mice. **P* < 0.05, ***P* < 0.01 vs. DMSO-treated wild-type adipocytes. The difference was determined using a one-way ANOVA. *Post hoc* analysis was performed using Dunnett's test. *Prdm16*: PR domain containing 16, *Cidea*: cell death-inducing DFFA-like effector A, *Elovl3*: fatty acid elongase 3.

Figure 5—Glucoraphanin alleviates HFD-induced hepatic steatosis and oxidative stress. *A*: Livers of mice fed the indicated diet for 14 weeks. Scale bar, 100 μ m. Bar graphs represent the liver weights (n = 9/group). *B*: H&E staining (original magnification, \times 200; scale bars, 100 μ m). *C*: Plasma ALT (left panel) and AST levels (right panel). *D*: Liver triglyceride (left panel) and FFA content (right panel). *E*: Quantitative real-time PCR determination of hepatic mRNA expression of genes involved in fatty acid synthesis, NADPH oxidase complex, antioxidant stress response, and fatty acid β -oxidation (normalized against *36B4*). *F*: Hepatic levels of malondialdehyde. Results represent mean \pm SEM. **P* < 0.05, ***P* < 0.01 vs. NC; #*P* < 0.05, ###*P* < 0.01 vs. HFD. ALT: alanine transaminase, AST: aspartate transaminase, TG: triglyceride, FFAs: free fatty acids, Cat: catalase, Gpx1: glutathione peroxidase 1, Sod1: superoxide dismutase 1, Ppara: peroxisome proliferator-activated

receptor α , Cpt1a: carnitine palmitoyltransferase 1a.

Figure 6—Glucoraphanin improves liver inflammation in HFD-fed mice. *A*: Relative mRNA expression of tumor necrosis factor- α (*Tnf- α*), chemokine (C-C motif) ligand 2 (*Ccl2*), and chemokine (C-C motif) receptor 2 (*Ccr2*) in the liver of mice fed the indicated diet for 14 weeks ($n = 8/\text{group}$). *B*: Immunoblot analysis of p-JNK (Thr¹⁸³/Tyr¹⁸⁵), JNK, p-Erk (Thr²⁰²/Tyr²⁰⁴), Erk, p-NF- κ B p65 (Ser⁵³⁶), and NF- κ B p65 using liver lysates. Each lane represents a liver lysate from a different animal ($n = 8/\text{group}$). Bar graphs represent normalized data of p-JNK/JNK, p-Erk/Erk, and p-NF- κ B p65/NF- κ B p65 from two independent experiments, presented as mean \pm SEM. *C*: Relative mRNA expression of macrophage markers. *D*: FACS analysis of macrophages in the liver of mice fed a HFD or HFD-GR diet ($n = 8/\text{group}$). Macrophages are defined as propidium iodide-CD45⁺NK1.1⁻CD3⁻CD19⁻TER119⁻CD11b⁺F4/80⁺ cells. Bar graph shows the number of liver macrophages. *E*: M1-like and M2-like macrophages are defined as CD11c⁺CD206⁻ and CD11c⁻CD206⁺, respectively. Bar graphs show the percentage of M1- and M2-like macrophages, and the M1/M2 ratio. Data are presented as mean \pm SEM. * $P < 0.05$, ** $P < 0.01$ vs. NC; # $P < 0.05$, ## $P < 0.01$ vs. HFD. A.U.: arbitrary unit.

Figure 7—Glucoraphanin decreases circulating lipopolysaccharide (LPS) and Gram-negative Proteobacteria in the gut microbiomes of HFD-fed mice. *A*: Plasma levels of LPS and LPS binding protein (LBP; *B*, left panel) in mice fed the indicated diet for 14 weeks ($n = 6-7/\text{group}$). Hepatic mRNA levels of *Lbp* (*B*, right panel) were determined by

quantitative RT-PCR. *C*: A principal component analysis was performed using the phylum-level taxonomic profiles of the cecal microbiota of the mice. Each plot represents the taxonomic profile data of individual mice. White circles = NC; white triangles = NC-GR; black circles = HFD; black triangles = HFD-GR. The closer the spatial distance between the individual data, the more similar they are with respect to both axes (PC1 and PC2). *D*: Relative abundance distribution of operational taxonomic unit (OTU) sequences (96% level). Percentage of total OTU sequences taxonomically assigned to bacterial phyla from cecal contents of mice fed the abovementioned diets for 14 weeks. *E*: Relative abundance of OTU sequences assigned to Proteobacteria phyla are shown as box plots. *F*: Relative abundance of OTU sequences assigned to Desulfovibrionaceae family is shown as box plots. Data are presented as mean \pm SEM (n = 6–7/group). * $P < 0.05$, ** $P < 0.01$ vs. NC; # $P < 0.05$ vs. HFD. *G*: Plasma LPS levels plotted against the relative abundance of the Desulfovibrionaceae family in the cecal contents. *H*: Correlations between plasma LPS and hepatic mRNA expression levels of TNF- α , gp91^{phox}, and F4/80. Inset corresponds to Spearman's r correlation and corresponding P value.

Figure 1

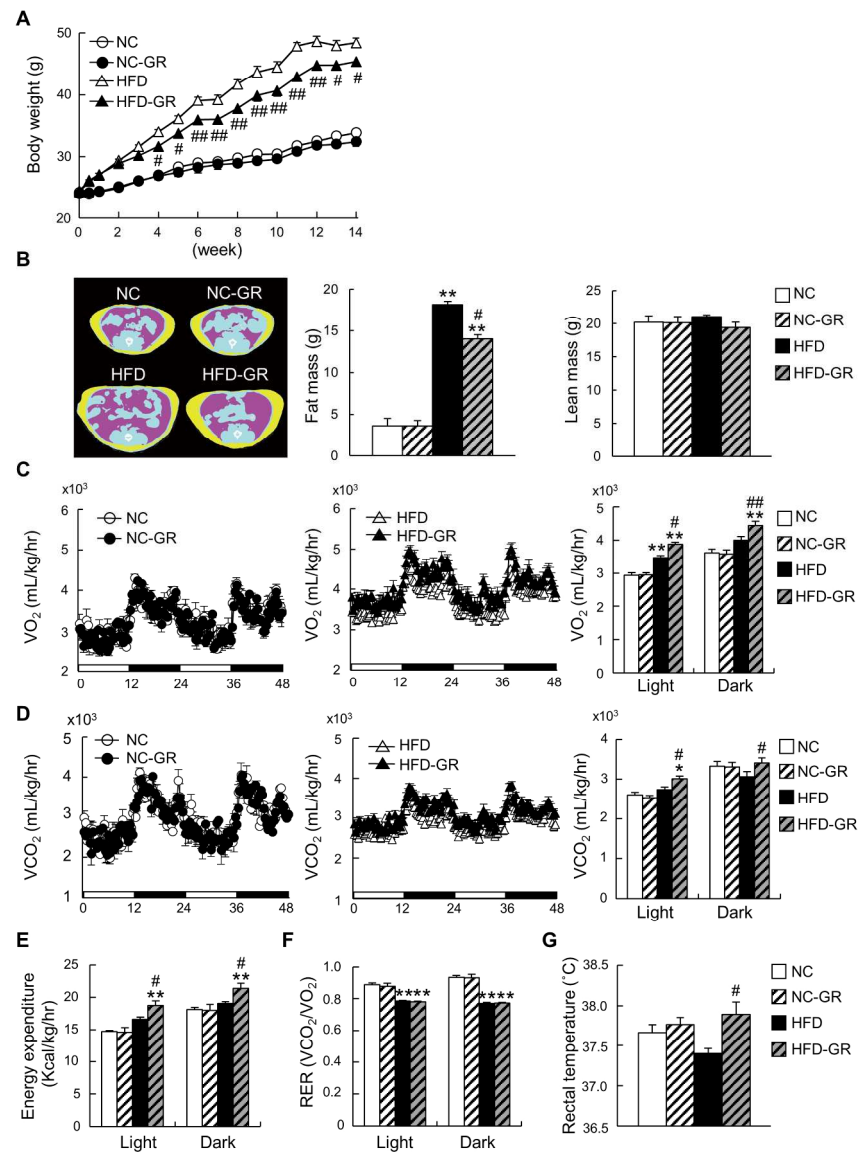


Figure 1

180x250mm (300 x 300 DPI)

Figure 2

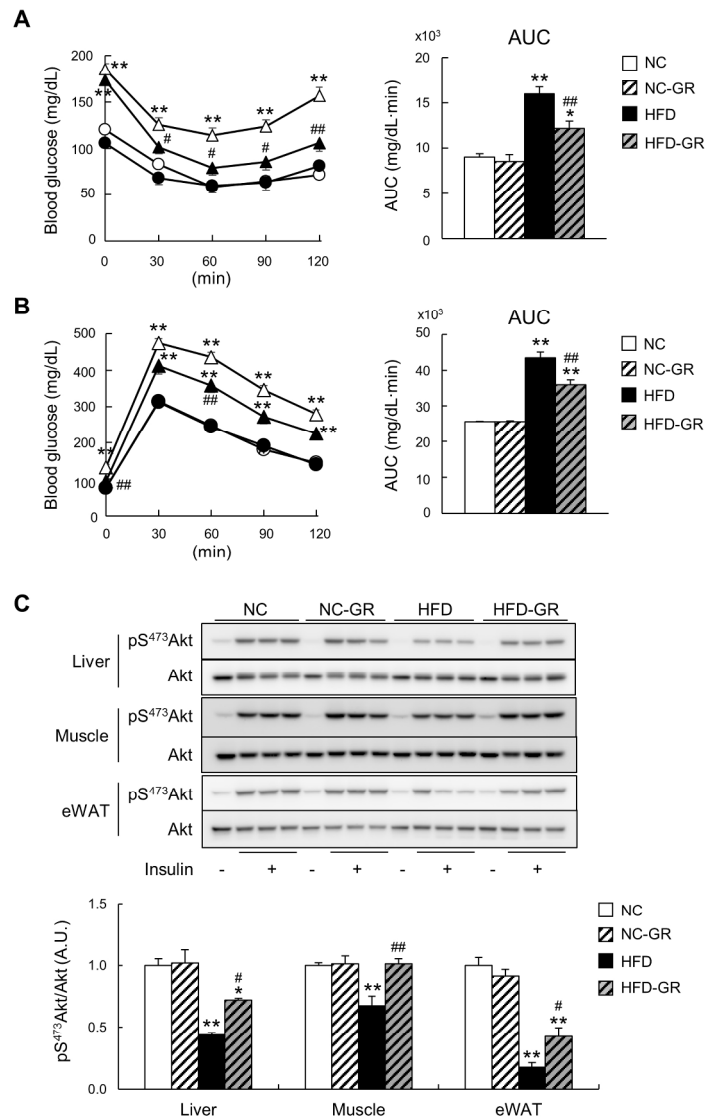


Figure 2

180x250mm (300 x 300 DPI)

Figure 3

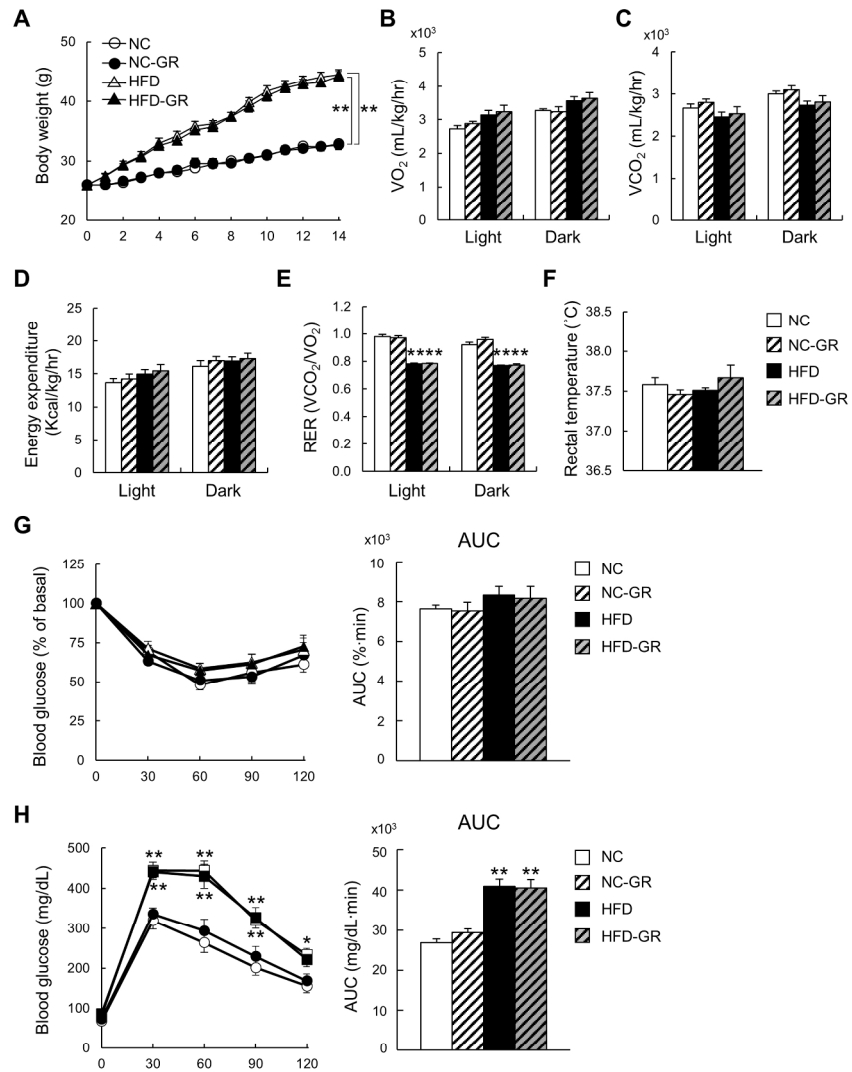


Figure 3

180x250mm (300 x 300 DPI)

Figure 4

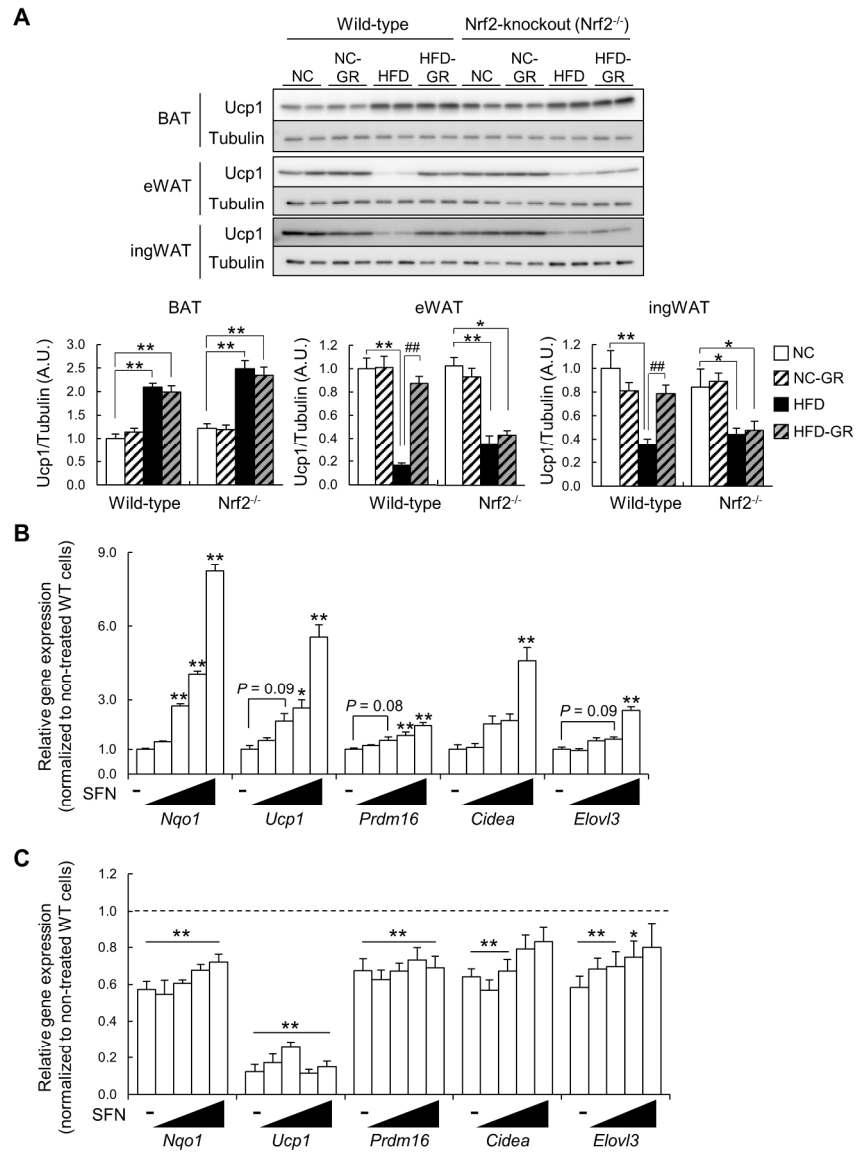


Figure 4

180x250mm (300 x 300 DPI)

Figure 5

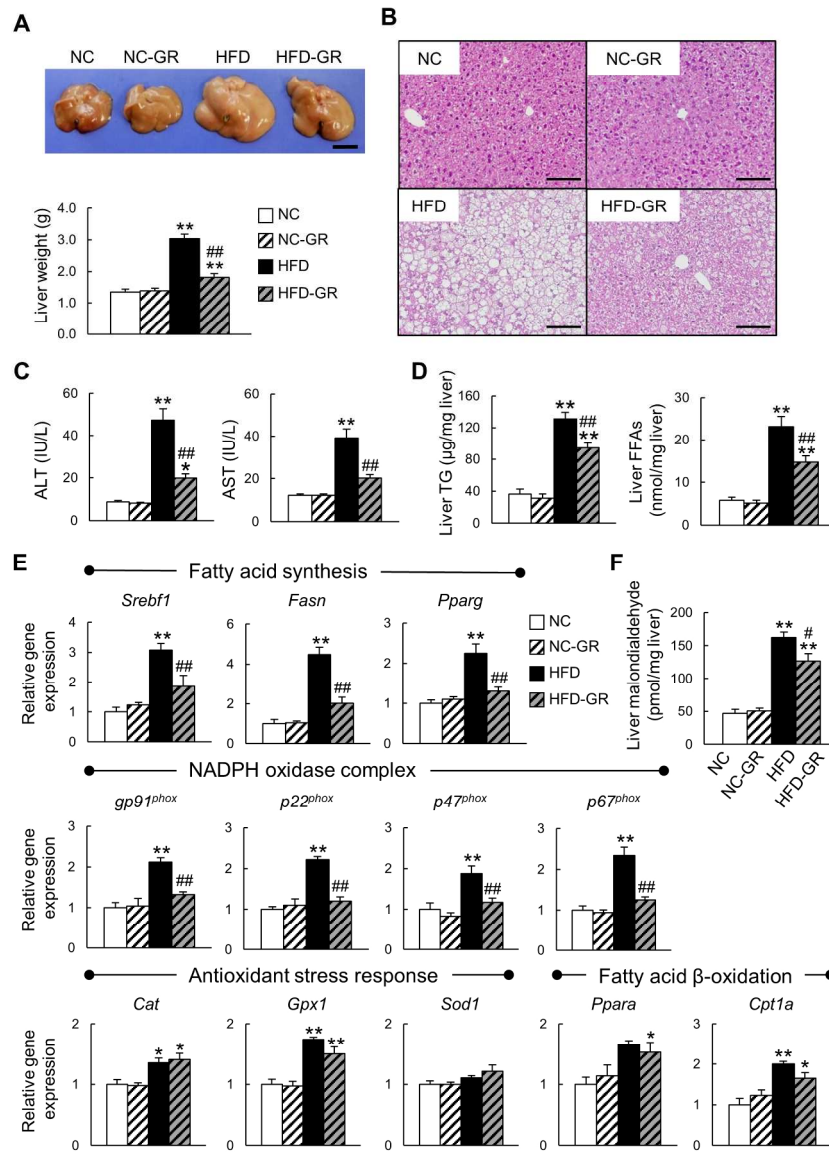


Figure 5

180x250mm (300 x 300 DPI)

Figure 6

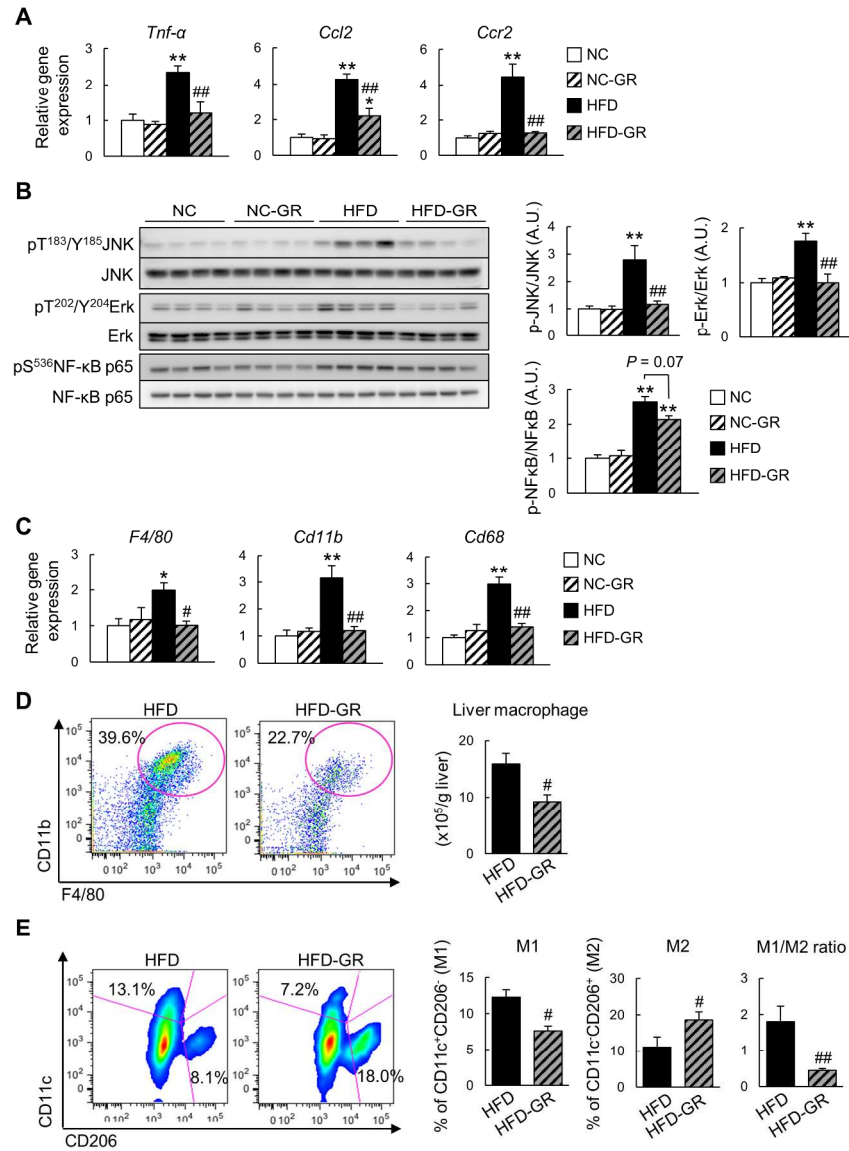


Figure 6

180x250mm (300 x 300 DPI)

Figure 7

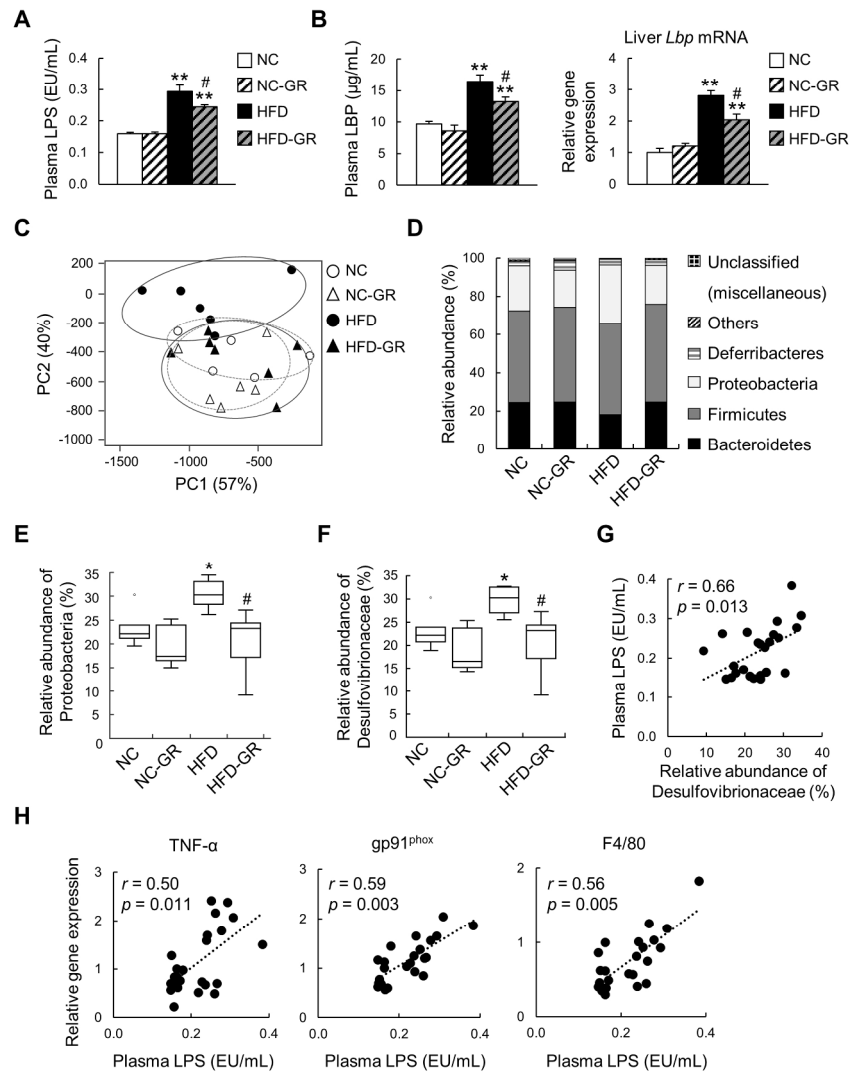


Figure 7

180x250mm (300 x 300 DPI)

Supplementary Table 1: Antibodies used for immunoblotting and FACS analysis.

Antibodies	Supplier
pS ⁴⁷³ Akt	Cell Signaling Technology #9271
Akt	Cell Signaling Technology #9272
pS ⁷⁹ -ACC	Cell Signaling Technology #3661
ACC	Cell Signaling Technology #3662
pT ¹⁷² -AMPK α	Cell Signaling Technology #2531
AMPK α	Cell Signaling Technology #2532
pT ²⁰² /Y ²⁰⁴ Erk1/2	Cell Signaling Technology #9101
Erk1/2	Cell Signaling Technology #9102
pT ¹⁸³ /Y ¹⁸⁵ JNK	Cell Signaling Technology #9255
JNK	Cell Signaling Technology #9258
pS ⁵³⁶ NF- κ B p65	Cell Signaling Technology #3033
NF- κ B p65	Cell Signaling Technology #3034
Tubulin	Cell Signaling Technology #2128
Ucp1	Abcam ab10983
PerCP-Cyanine5.5-conjugated NK1.1	eBioscience #45-5941
PerCP-Cyanine5.5-conjugated CD3	eBioscience #45-036

PerCP-Cyanine5.5-conjugated CD19	eBioscience #45-0193
PerCP-Cyanine5.5-conjugated TER-119	eBioscience #45-5921
Allophycocyanin-eFluor 780-conjugated CD45	eBioscience #47-0451
Phycoerythrin-conjugated CD11c	eBioscience #12-0114
eFluor 450-conjugated Ly-6G (Gr-1)	eBioscience #48-5931
PE/Cy7-conjugated F4/80	Biolegend #123113
Alexa Fluor 647-conjugated CD206	Biolegend #141712
PE-Texas Red-conjugated CD11b	Invitrogen #RM2817

Supplementary Table 2: Primers used for quantitative RT-PCR.

Gene/Primer	Forward	Reverse
Catalase	CCAGCGACCAGATGAAGCAG	CCACTCTCTCAGGAATCCGC
Ccl2	AGGTCCCTGTCATGCTTCTGG	CTGCTGCTGGTGATCCTCTTG
Ccr2	ATTCTCCACACCCTGTTTCG	GATTCCTGGAAGGTGGTCAA
CD11b	CATCAAGGGCAGCCAGATTG	GAGGCAAGGGACACACTGAC
CD11c	AAAATCTCCAACCCATGCTG	CACCACCAGGGTCTTCAAGT
CD68	CTTCCCACAGGCAGCACAG	AATGATGAGAGGCAGCAAGAGG
Cidea	TGCTCTTCTGTATCGCCCAGT	GCCGTGTTAAGGAATCTGCTG
Cpt1a	AAACCCACCAGGCTACAGTG	TCCTTGTAATGTGCGAGCTG
Dio2	CTTCTGAGCCGCTCCAAGTC	CACCCAGTTTAACCTGTTTGTAGG
Elovl3	TCCGCGTTCTCATGTAGGTCT	GGACCTGATGCAACCCTATGA
F4/80	CTTTGGCTATGGGCTTCCAGTC	GCAAGGAGGACAGAGTTTATCGTG
Fasn	AGAGACGTGTCACTCCTGGACTT	GCTGCGGAAACTTCAGAAAAT
Fabp4	GGGGCCAGGCTTCTATTCC	GGAGCTGGGTTAGGTATGGG
gp91 ^{phox}	TTGGGTCAGCACTGGCTCTG	TGGCGGTGTGCAGTGCTATC
Gpx1	TTCGGACACCAGGAGAATGG	TAAAGAGCGGGTGAGCCTTC
Hmox1	CAGAGCCGTCTCGAGCATAG	CAAATCCTGGGGCATGCTGT

Lbp	GTCCTGGGAATCTGTCCTTG	CCGGTAACCTTGCTGTTGTT
Nqo1	CTCTGGCCGATTCAGAGTGG	CTCCCAGACGGTTTCCAGAC
p22 ^{phox}	GTCCACCATGGAGCGATGTG	CAATGGCCAAGCAGACGGTC
p47 ^{phox}	GATGTTCCCCATTGAGGCCG	GTTTCAGGTCATCAGGCCGC
p67 ^{phox}	CTGGCTGAGGCCATCAGACT	AGGCCACTGCAGAGTGCTTG
Ppara α	GAGGGTTGAGCTCAGTCAGG	GGTCACCTACGAGTGGCATT
Ppar γ	GAAACTCTGGGAGATTCTCCT	CAGAGCTGATTCCGAAGTTGG
Ppargc1a	ATGTGTCGCCTTCTTGCTCT	ATCTACTGCCTGGGGACCTT
Prdm16	CAGCACGGTGAAGCCATTC	GCGTGCATCCGCTTGTG
Prdx1	TGTCCCACGGAGATCATTGC	GGGTGTGTTAATCCATGCCAG
Sod1	CAGCATGGGTTCCACGTCCA	CACATTGGCCACACCGTCCT
Srebf1	GGAGCCATGGATTGCACATT	GGCCCGGGAAGTCACTGT
Tnfa	CCCACACCGTCAGCCGATTT	GTCTAAGTACTTGGGCAGATTGACC
Ucp1	ACTGCCACACCTCCAGTCATT	CTTTGCCTCACTCAGGATTGG
Ucp2	ATGGTTGGTTTCAAGGCCACA	CGGTATCCAGAGGGAAAGTGAT
Ucp3	CTGCACCGCCAGATGAGTTT	ATCATGGCTTGAAATCGGACC

Supplementary Table 3: Metabolic parameters of *Nrf2*^{-/-} mice.

	NC (n = 8)	NC-GR (n = 8)	HFD (n = 11)	HFD-GR (n = 7)
Plasma TG (mg/dL)	99 ± 11	102 ± 11	114 ± 11	131 ± 15
Plasma TC (mg/dL)	143 ± 25	152 ± 23	187 ± 18	199 ± 21
Plasma FFAs (mmol/L)	1.4 ± 0.1	1.3 ± 0.1	1.1 ± 0.1*	1.0 ± 0.1**
Blood glucose (mg/dL)				
Fed	158 ± 7	161 ± 6	191 ± 8**	176 ± 6
Fasted	65 ± 3	68 ± 4	100 ± 6**	98 ± 5**
Plasma insulin (ng/mL)				
Fed	2.2 ± 0.3	2.1 ± 0.3	9.6 ± 2.5	7.2 ± 2.1
Fasted	0.5 ± 0.1	0.5 ± 0.1	1.3 ± 0.1**	1.7 ± 0.2**
HOMA-IR	2.0 ± 0.4	2.0 ± 0.5	9.2 ± 1.1**	10.7 ± 1.7**
Plasma ALT (IU/L)	14.5 ± 1.8	13.8 ± 2.0	47.8 ± 6.6**	44.7 ± 4.7**
Plasma AST (IU/L)	52.7 ± 4.2	50.2 ± 3.9	105.4 ± 9.0**	105.1 ± 15.4**

Shown are blood glucose and plasma insulin levels of mice fed (ad libitum) or fasted for 16

h. Plasma triglyceride (TG), total cholesterol (TC), and free fatty acids (FFAs) were measured in fasting plasma. Measurements are reported as mean ± SEM. **P* < 0.05, ***P* < 0.01 vs. NC. NC: normal chow, HFD: high-fat diet, GR: glucoraphanin, HOMA-IR: homeostasis model assessment of insulin resistance, ALT: alanine transaminase, AST:

aspartate transaminase.

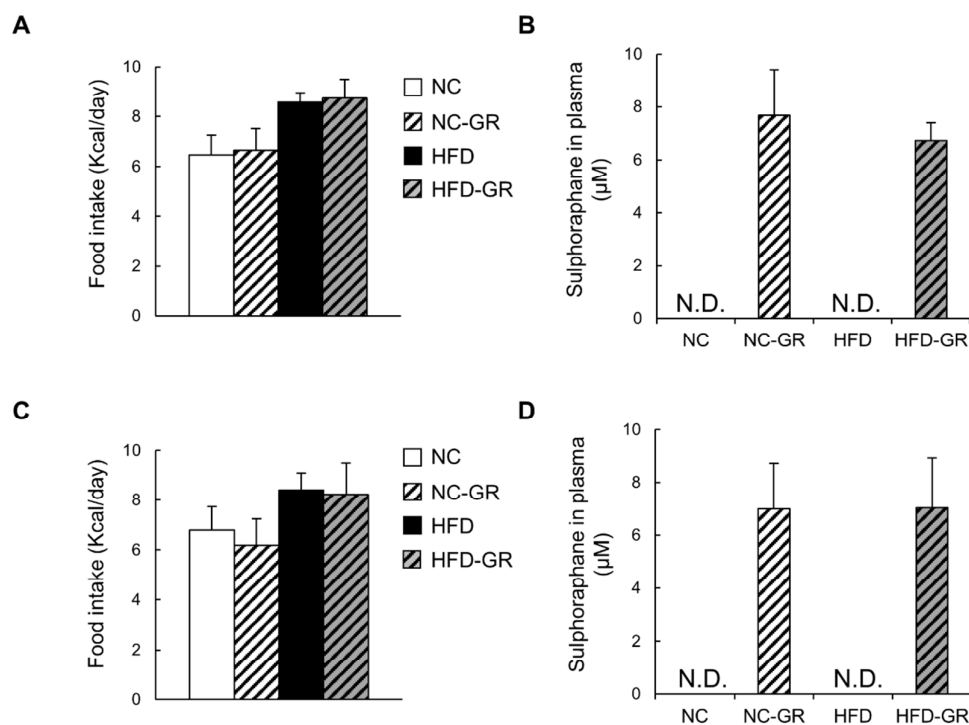
Supplemental Table 4: Metabolic endotoxemia positively correlated with mRNA expression of genes involved in inflammation, oxidative stress, and macrophage infiltration in the liver.

		Inflammation				Oxidative stress				Macrophage infiltration		
	LPS	Tnf- α	Il-1 β	Ccl2	Ccr2	gp91 ^{phox}	p22 ^{phox}	p47 ^{phox}	p67 ^{phox}	F4/80	Cd11b	Cd68
LPS	1											
Tnf- α	0.44*	1										
Il-1 β	0.47*	0.55**	1									
Ccl2	0.64**	0.76**	0.54**	1								
Ccr2	0.55**	0.56**	0.65**	0.75**	1							
gp91 ^{phox}	0.59**	0.66**	0.74**	0.80**	0.69**	1						
p22 ^{phox}	0.47*	0.70**	0.64**	0.72**	0.53*	0.94**	1					

p47 ^{phox}	0.58**	0.61**	0.84**	0.55**	0.58**	0.89**	0.86**	1				
p67 ^{phox}	0.65**	0.67**	0.72**	0.72**	0.69**	0.83**	0.87**	0.85**	1			
F4/80	0.51*	0.53**	0.67**	0.51*	0.51*	0.85**	0.90**	0.87**	0.81**	1		
Cd11b	0.57**	0.60**	0.60**	0.70**	0.50*	0.88**	0.84**	0.71**	0.77**	0.78**	1	
Cd68	0.53*	0.68**	0.64**	0.79**	0.50*	0.91**	0.90**	0.67**	0.69**	0.63**	0.90**	1

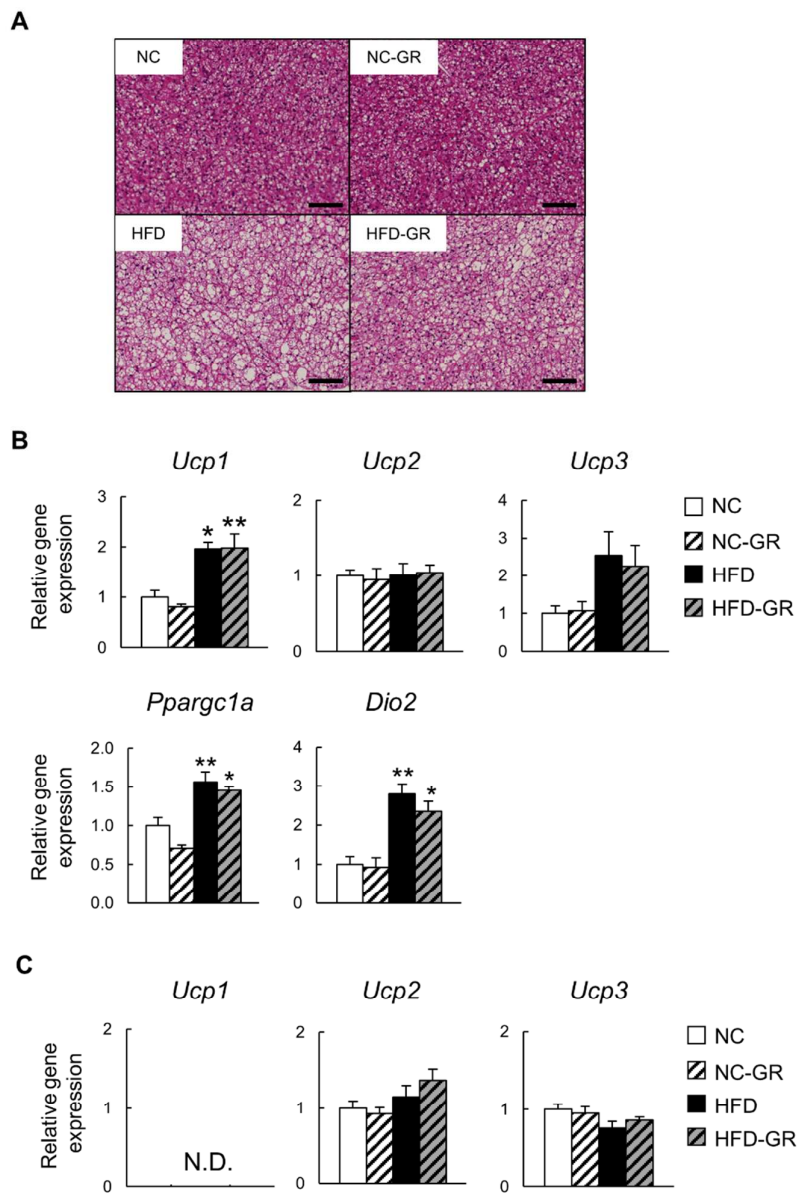
Values correspond to Spearman's r correlation. * $P < 0.05$, ** $P < 0.01$

Supplementary Figure 1



Supplementary Figure 1—**A**: Food intake of wild-type mice fed normal chow (NC), chow with glucoraphanin (NC-GR), a high-fat diet (HFD), or HFD with GR (HFD-GR) was measured after 3 weeks of feeding. Data are presented as the mean \pm SEM ($n = 9/\text{group}$). **B**: Plasma concentration of sulforaphane in wild-type mice fed the indicated diet for 6 weeks. Data are presented as the mean \pm SEM ($n = 3/\text{group}$). **C**: Food intake of $\text{Nrf2}^{-/-}$ mice fed the indicated diet after 3 weeks. Data are presented as the mean \pm SEM ($n = 7\text{--}11/\text{group}$). **D**: Plasma concentration of sulforaphane of $\text{Nrf2}^{-/-}$ mice fed the indicated diet for 6 weeks. Data are presented as the mean \pm SEM ($n = 5\text{--}6/\text{group}$).

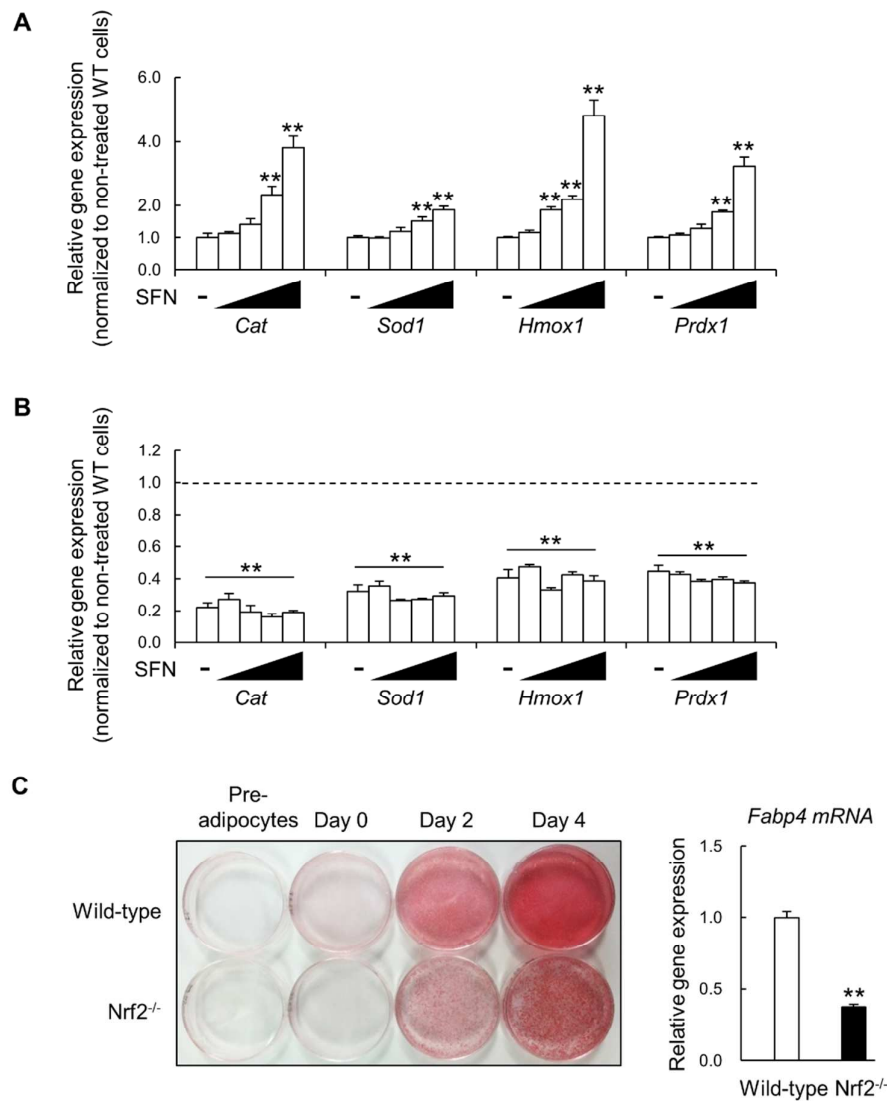
Supplementary Figure 2



Supplementary Figure 2—A: H&E staining of brown adipose tissue of mice fed the indicated diet for 14 weeks (original magnification, $\times 200$; scale bars, 100 μm). B: Relative mRNA expression of genes implicated in uncoupling proteins (*Ucp-1*, *Ucp-2*, and *Ucp-3*), PGC-1 α (*Ppargc1a*), and Deiodinase 2 (*Dio2*) in the brown adipose tissue

of mice fed the indicated diet for 14 weeks (n = 8/group). C: Relative mRNA expression of genes implicated in uncoupling proteins in quadriceps muscle of mice fed the indicated diet for 14 weeks. Results represent the mean \pm SEM (n = 8/group). * P < 0.05, ** P < 0.01 vs. NC. N.D., not detected.

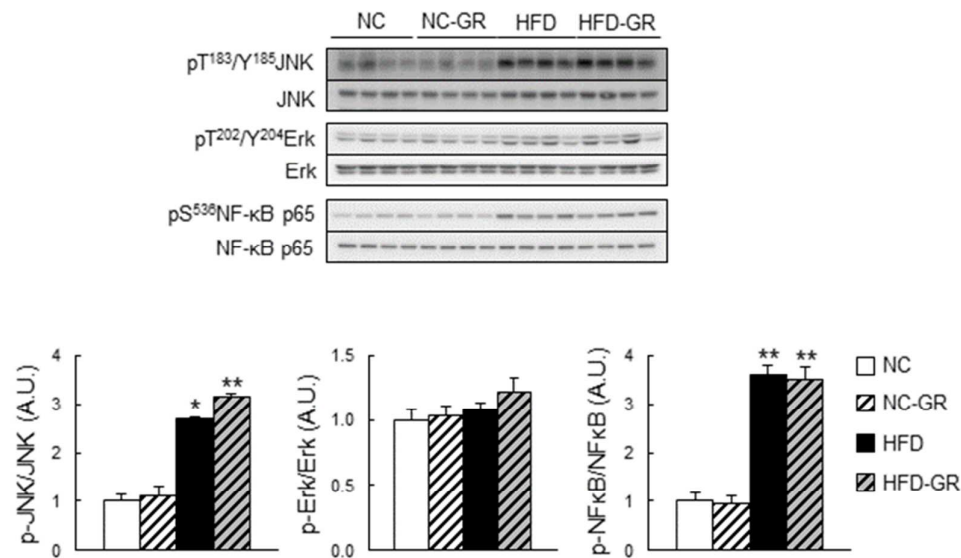
Supplementary Figure 3



Supplementary Figure 3—Stromal vascular fraction cells were grown to confluence, then differentiation was induced as described in Methods. *A*: Quantitative real-time PCR determination of mRNA levels of Nrf2 target antioxidant genes in the absence or presence of sulforaphane (SFN; 0.2, 1, 2, or 5 μ M) for 48 h in primary beige adipocytes isolated from inguinal WAT of wild-type mice (normalized against 36B4). *B*: The same

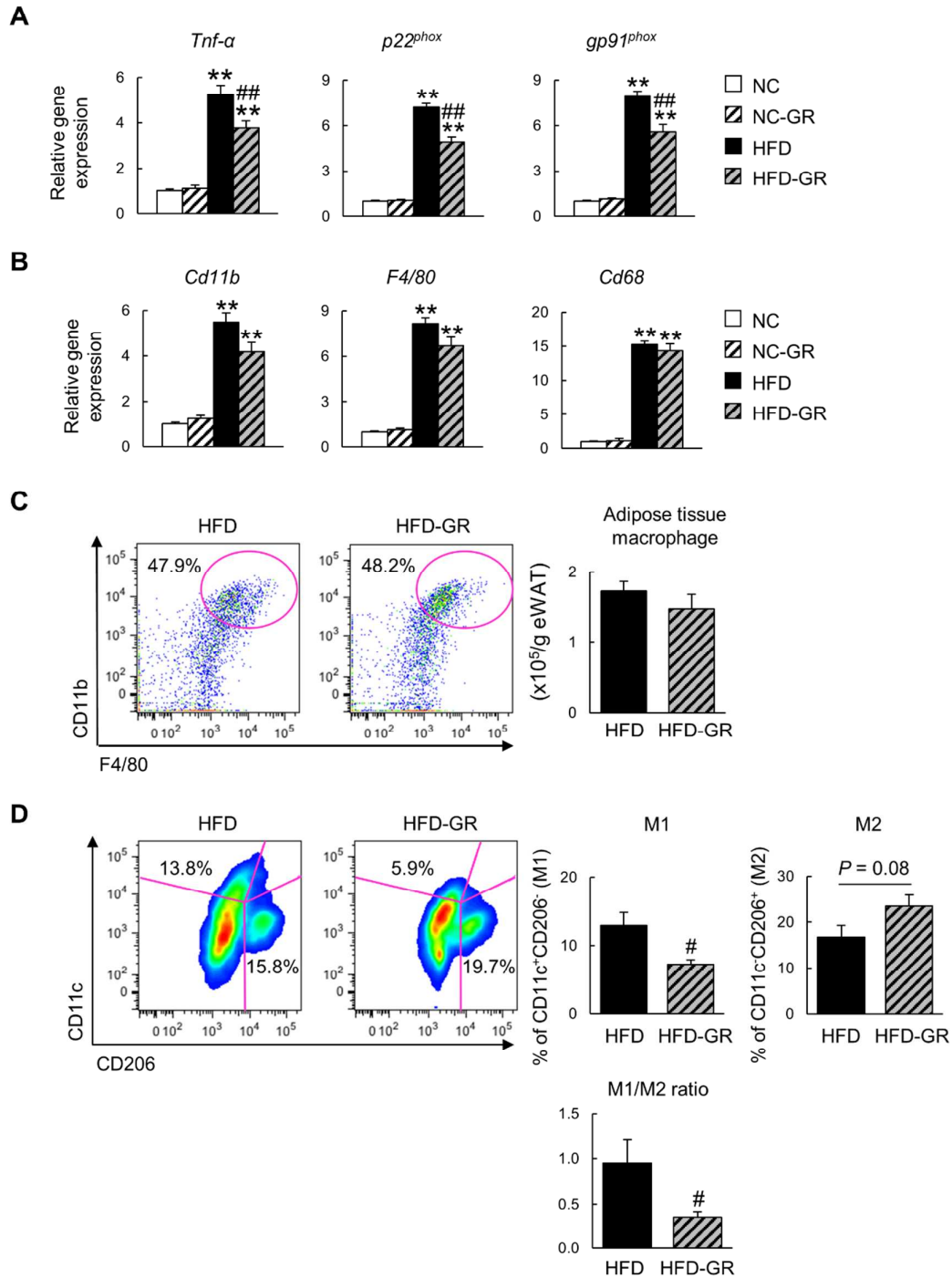
experiment as in (A) was repeated with primary beige adipocytes isolated from inguinal WAT of *Nrf2*^{-/-} mice. Bar graphs represent mean \pm SEM (n = 6/group). **P* < 0.05, ***P* < 0.01 vs. DMSO-treated adipocytes from wild-type mice. The difference was determined using a one-way ANOVA. Post hoc analysis was performed using Dunnett's test. Cat: catalase, Sod1: superoxide dismutase 1, Hmox1: heme oxygenase 1, Prdx1: peroxiredoxin 1. C (left panel): At various stages of differentiation, cells were fixed and stained with oil red O. C (right panel): Quantitative real-time PCR determination of mRNA levels of adipocyte differentiation marker, fatty acid binding protein 4 (*Fabp4*), in wild-type and *Nrf2*-deficient beige adipocytes after 7 days of culture with maintenance medium. Bar graphs represent mean \pm SEM (n = 6/group). ***P* < 0.01 vs. wild-type adipocytes.

Supplementary Figure 4



Supplementary Figure 4—Immunoblot analysis of p-JNK (Thr183/Tyr185), JNK, p-ERK (Thr202/Tyr204), ERK, p-NF-κB p65 (Ser536), and NF-κB p65 using liver lysates of *Nrf2*^{-/-} mice fed the indicated diet for 14 weeks. Each lane represents a liver lysate from a different animal (n = 8/group). Bar graphs represent normalized data of p-JNK/JNK, p-Erk/Erk, and p-NF-κB p65/ NF-κB p65 from two independent experiments, presented as mean ± SEM. **P* < 0.05, ***P* < 0.01 vs. NC. A.U.: arbitrary unit.

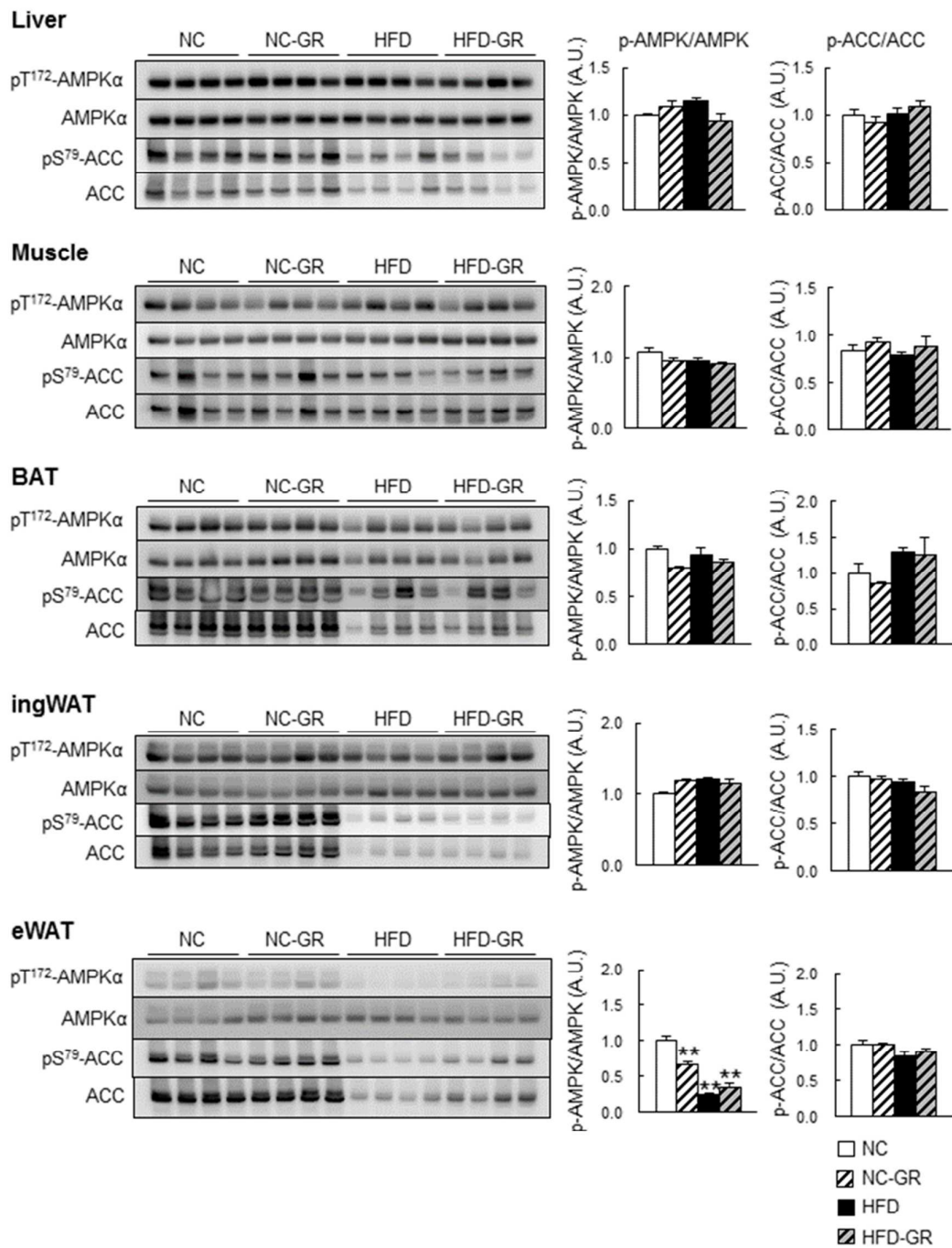
Supplementary Figure 5



Supplementary Figure 5— Relative mRNA expression of genes implicated in (A) *Tnf-α*, *p22^{phox}*, and *gp91^{phox}*, and (B) cell surface markers for macrophage, including *Cd11b*,

F4/80, and *Cd68* in the epididymal white adipose tissue (eWAT) of mice fed the indicated diet for 14 weeks. *C*: FACS analysis of macrophage in eWAT of mice fed HFD or HFD-GR diet. Macrophages are defined as propidium iodide-CD45+NK1.1-CD3-CD19-TER119-CD11b+F4/80+ cells. Bar graphs show the number of macrophages in eWAT. *D*: M1-like and M2-like macrophages are defined as CD11c+CD206- and CD11c-CD206+ cells, respectively. Bar graphs show the percentage of M1- and M2-like macrophages, and the M1/M2 ratio. Data are presented as mean \pm SEM (n = 8/group). *P < 0.05, **P < 0.01 vs. NC; #P < 0.05, ##P < 0.01 vs. HFD.

Supplementary Figure 6



Supplementary Figure 6—Immunoblot analysis of p-AMPK α (Thr172), AMPK α , p-ACC (Ser79), and ACC using lysates of liver, quadriceps muscles, intrascapular

brown adipose tissue (BAT), inguinal white adipose tissue (ingWAT), and epididymal WAT (eWAT) from mice on the indicated diet for 14 weeks. Bar graphs represent normalized data of p-AMPK/AMPK α and p-ACC/ACC from two independent experiments, presented as mean \pm SEM (n = 8/group). ***P* < 0.01 vs. NC. A.U., Arbitrary unit.